SCLC TumorMiner: A Genomics Platform for Small Cell Lung Cancer Precision Oncology

Fathi Elloumi[1,*,#], Anjali Dhall[1,*], Daiki Taniyama[1], Augustin Luna[1,2], Yasuhiro Arakawa[1,3], Sudhir Varma[1,4], Yanghsin Wang[1,5], Anisha Tehim[1,6], Mark Raffeld [7], Kenneth Aldape[7], Christophe Redon[1], Roshan Shresta[1], William Reinhold[1], Mirit Aladjem[1], Jaydira Del Rivero[1], Nitin Roper[1], Anish Thomas[1] and Yves Pommier[1,#]

[1]Laboratory of Molecular Pharmacology and Developmental Therapeutics Branch, Center for Cancer Research, NCI, NIH
[2]National Library of Medicine (NLM), NIH
[3]Department of Clinical Pharmacology and Therapeutics, The Jikei University School of Medicine, Tokyo, Japan
[4]HiThru Analytics LLC
[5]Essex Management, LLC, An Emmes Company
[6]Cornell University, NY
[7]Laboratory of Pathology, Center for Cancer Research, NCI, NIH

[*] Equal contributions
[#] To whom correspondence should be addressed: pommier@nih.gov; fathi.Elloumi@nih.gov

SUMMARY

Small cell lung cancer (SCLC) is among the most aggressive malignancies. Unlike many other cancers, it is not represented in The Cancer Genome Atlas, and available datasets are fragmented across institutions, disease stages, and treatment settings. RNA sequencing provides a powerful and cost-effective approach, but the high dimensionality of transcriptomic data and the heterogeneity of patient cohorts pose significant challenges. To address such challenges, we developed SCLC TumorMiner (https://discover.nci.nih.gov/SclcTumorMinerCDB/), which includes 50 tumor samples from relapse patients at the National Cancer Institute (NCI) and 154 samples from untreated patients at the University of Cologne and Tongji University. SCLC TumorMiner enables molecular classification, genomic pathway analyses, risk stratification, identification of predictive cell-surface biomarkers such as DLL3 or TROP2, and drug-response biomarkers such as SLFN11. SCLC TumorMiner illustrates profound differences between untreated and relapse patient samples. Additionally, "MyPatient", one of SCLC TumorMiner's modules, is presented as a medical assistant application prototype.

INTRODUCTION

Small cell lung cancers are rapidly proliferative tumors often diagnosed with metastases (Extensive-stage; ES-SCLC) [1]. They account for approximately 13%–15% of all lung cancer cases and remain one of the most lethal malignancies. Survival is less than one year for most patients, and 95% of patients die within 5 years despite initial response to cisplatin-etoposide combination therapy. Upon relapse, tumors evolve and become resistant to chemotherapy, reflecting profound changes in their biology and genomic network.

In addition to mutations of the tumor suppressors TP53 and RB1 in 80% of SCLC, selective activation of transcription factors characterizes the disease [2,3]. At diagnosis, SCLCs have been divided into two groups. 70-80% are neuroendocrine (NE), driven by two pioneer neurogenic transcription factors, ASCL1 (Acheate-scute homolog 1) and NEUROD1 (Neurogenic differentiation factor 1). The remaining non-NE SCLCs are driven by two other transcription factors POU2F3 (POU class 2 homeobox 3) and YAP1 (Yes-associated protein 1). Consequently, SCLCs have been classified into 4 subsets: SCLC-A, SCLC-N, SCLC-P, and SCLC-Y [3] (NAPY classification [3,4]). Additionally, an Inflamed/Immune subgroup has been identified as SCLC-I [5]. These classifications are well supported in untreated tumors and SCLC cell lines [3,4] (see Figure 1B), but are not routinely applied in clinical practice, where diagnosis and classification rely primarily on neuroendocrine marker immunohistochemistry for synaptophysin (encoded by the *SYP* gene), chromogranin (encoded by *CHGA*), and neural cell adhesion molecule (encoded by *NCAM1*).

Immune checkpoint (PD-L1) inhibitors added to chemotherapy are the standard of care for first-line treatment of ES-SCLC [6,7]. However, they only provide a modest overall survival benefit of 2-3 months [7,8]. A recent therapeutic breakthrough for SCLC is Tarlatamab®, a bispecific T-cell engager (BiTE®) targeting the Notch ligand cell surface glycoprotein DLL3 (Delta-like ligand 3), a transcriptional target of ASCL1 [4]. However, responses are heterogeneous, and Tarlatamab® is currently administered without mandatory biomarker-based patient selection.

In parallel, antibody–drug conjugates (ADCs) and CAR-T therapies targeting surface antigens such as DLL3, TROP2 (anti-trophoblast antigen 2 encoded by *TACSTD2*), SEZ6 (seizure 6-like), carcinoembryonic antigen–related cell adhesion molecules (CEACAM5 and CEACAM6), and B7-H3 (member of the B7-cell family homolog 3 encoded by *CD276*) are actively being developed. For ADCs in particular, therapeutic efficacy depends not only on target expression but also on payload sensitivity, including replication stress–associated vulnerabilities such as expression of Schlafen 11 (SLFN11) and Ki67 (encoded by *MKI67*).

With the advancement of high-throughput genomic sequencing methods, bulk RNA sequencing (RNA-seq) has emerged as a well-established, sensitive, and clinically usable method for transcriptome analyses. However, even when only applied to protein-coding genes, it generates around 20,000 gene expression data per sample, which are difficult to analyze instantaneously in a clinical setting. To address this challenge, we developed SCLC TumorMiner, integrating 204 SCLC patient samples. Fifty samples are collected from patients at relapse in our NCI clinic, and 154 are from the published datasets of untreated patients from the University of Cologne (UoC) [2] and Tongji University (TU) [9] (Table 1, Table S1). The architecture and interface of TumorMiner is based on our SCLC CellMinerCDB website comprising the genomics and drug responses of 118 SCLC cell lines (https://discover.nci.nih.gov/SclcCellMinerCDB) [4]. Thus, SCLC TumorMiner and SCLC-CellMinerCDB can be readily used to compare tumor samples with cell lines.

Here we provide a tutorial and demonstrate how SCLC TumorMiner allows instantaneous: 1/ Transcriptome and mutations analyses of patient samples; 2/ Molecular pathway analyses; 3/ Patient sample classification based on NAPY and/or NMF (non-negative matrix factorization); and 4/ Identification of prognosis and predictive biomarkers for targeted therapies.

RESULTS

Introduction to SCLC TumorMiner and brief tutorial

SCLC TumorMiner uses the same architecture as our six-cancer cell line CellMiner websites (https://discover.nci.nih.gov/). Thus, users familiar with SCLC-CellMinerCDB (https://discover.nci.nih.gov/SclcCellMinerCDB/) will have no difficulty navigating back and forth between the tumor samples and cell lines databases [4].

Figure 1 (https://discover.nci.nih.gov/SclcTumorMinerCDB/) introduces the website as a snapshot of the default page display. The upper part shows the tabs for each of the tools and applications. They are numbered 1-10 for convenience on the figure. The "2 variable Analyses" tab (numbered "1" in Figure 1A) allows the display of different data types or parameters on each of the axes: "xsq" (RNA-seq), "sig" (Signatures), "mut" (gene mutations), "mda" (Miscellaneous data), "hll" (Hallmark gene sets) and "act" (Drug Response). For instance, plotting ASCL1 expression vs. NE (Neuro Endocrine) signature (Figure S1A) shows their expected high correlation within each of the 3 datasets (NCI, UoC, TU).

2-Variable Analysis data can be downloaded as Tab-delimited files for further exploration. Figure 1B compares the expression of *NEUROD1*, *ASCL1*, *POU2F3* and *YAP1* across datasets. It demonstrates the reduced *ASCL1* and *POU2F3* expression associated with increased *YAP1* expression in the relapse samples (Figure 1A). As a result, the assignment of samples to each of the NAPY groups can only be applied to 44% of the relapse samples while, it discriminates all the samples from untreated patients [3] and 92% of the cell lines from SCLC-CellMinerCDB [4] (Figure 1B).

The "Multivariable Analyses" tab (labeled "2" in Figure 1A) shows as default display the heatmap of *ASCL1* expression (xsq: RNA-seq) vs. the expression of key genes driving SCLC: *INSM1* & *CHGA* encoding immunohistochemistry NE markers, *MKI67* (encoding Ki67 used as proliferation marker), and the SCLC pioneer transcription factors *NEUROD1*, *POU2F3* & *YAP1*, and the oncogene *MYC* (Figure 2A). Each row displays the selected genes, and the columns represent each of the 204 individual patient samples. Users can explore different inputs and outputs by entering gene names in the "Response Identifier" or "Predictor Identifiers" windows (left panels of Figure 2A). Examples of "Multivariate Analyses" for the NAPY genes are shown in Figure 2A-E and will be discussed in the next section.

Under the "Multivariate Analyses" tab, in addition to the default visualization set up by default as "Display", users can choose the "Linear Regression" tab (found at the bottom left corner of the website under "Algorithm"; Figure 2A). This feature computes the correlation between each of the "Predictive Identifiers" and the "Response Identifier". Figure S2A-B shows the results for *ASCL1* for the genes entered in Figure 2B. The "Plot" and "Technical Details" options illustrate the highly significant value of the combined expression of *NKX2.1*, *FOXA2*, *DLL3* and *SEZ6* as predictors of *ASCL1* expression in the combined datasets (UoC and TU) of the untreated patients

124 (Figure S2A-B). Users can also choose "Lasso" (Least Absolute Shrinkage and Selection
125 Operator), a machine-learning and statistical method to identify genomic biomarkers predicting
126 the expression of "Response Identifiers". For *YAP1* expression, the top gene identified in the
127 relapse samples is the Neuron Restrictive Silencing Factor *REST*, a key effector of the Notch
128 pathway (Figure S2D) [4].

129 The "Expression Distribution" tab (labeled "3" in Figure 1A) displays the expression of
130 any chosen gene across the 3 datasets (the two untreated TU & UoC datasets and the relapse
131 patients from the NCI dataset). *SLFN11* expression is displayed as default on the website (Figure
132 S3A). Its reduced expression in the relapse samples is consistent with the resistance of relapsing
133 patients to DNA-targeted chemotherapies. Users can also display and download data for any gene
134 from each of the 3 datasets by typing the gene HUGO name in the "Gene symbol" box. Such
135 analyses for the housekeeping genes *GADPH*, *ACTB* (β-actin), or *B2M* (β2-macroglobulin) show
136 high expression and lack of significant expression differences between untreated and relapse
137 samples, suggesting limited batch effect for highly expressed genes (>5 in at least one dataset).

138 The "Mutation Variants" tab (labeled "4" in Figure 1A) displays up to 5 genes at a time.
139 Colors reflect the different types of mutations, including: Missense_Mutation,
140 Nonsense_Mutation, Frame_shift_Ins, Frame_Shit_Del, In_Frame_Del, Multi_Hit. Variants can
141 be viewed and downloaded with the "View variants" tab (Figure S3B). As expected, *TP53* is the
142 most frequently mutated gene (81% of the 114 samples with whole-exome sequencing data). The
143 second most frequently mutated gene is *TTN,* encoding Titin. This is not surprising as Titin is the
144 largest human protein and SCLC has a high mutation burden. RB1 shows an overall mutation
145 frequency of 55% (Figure S3B). By computing the copy number (Ploidy) values for RB1 for the
146 TU and NCI SCLC (114) samples and using an *ad hoc* rule (samples with < 0.05 ploidy for full
147 depletion and between 0.05 and 1.85 for partial depletion), percentages for full and partial
148 depletions are 62.8% and 17.7%, respectively (Table S2). Inactivation of SLFN11 was observed
149 in only 4% of samples (Figure S3B), consistent with epigenetic inactivation as the main
150 mechanism for suppressing SLFN11 expression and conferring chemoresistance [10].

151 The "Prognosis Biomarkers", "Predictive Biomarkers" and "MyPatient" tabs (numbered 5,
152 6 & 7 in Figure 1A) will be discussed in the remaining sections of the manuscript with examples
153 displayed in Figures 5 & 6.

154

155 **Genomic networks and pathway explorations**

156 We previously reported [4] in the SCLC cell lines, the expression of genes of a given pathway are
157 cross-correlated [see Fig. 5 in [4]]. The main pathways for SCLC comprise the neuroendocrine (NE)
158 pathways driven prominently by *ASCL1* and less frequently by *NEUROD1*, and the non-NE
159 pathways driven by *POU2F3* and *YAP1*, the *MYC* genes, and the Notch pathway [3,4]. As in the
160 SCLC cell lines (https://discover.nci.nih.gov/SclcCellMinerCDB/) [4], the group of NE-SCLC
161 prominently expresses *INSM1* and *CHGA,* encoding routinely used immunochemistry biomarkers
162 (Figure 2A). As expected, *ASCL1* expression is highly correlated with *INSM1* and *CHGA*. Figure
163 2A also shows that multiple samples express both *ASCL1* and *NEUROD1*, and a significant overlap
164 between *YAP1*, *POU2F3* and *MYC* expression.

165 Analysis of the *ASCL1* coexpression network in the samples from untreated patients
166 (Figure 2B) confirms [4] that most samples expressing *ASCL1* coexpress *INSM1* (highly significant

correlations in the "2 variable analysis"). As expected, the transcriptional coactivators of *ASCL1*, *NKX2-1* and *PROX1* [4,11] show coexpression (confirmed in the "2 variable analysis"). *DLL3*, the downstream transcriptional target of ASCL1, is highly expressed in approximately two-third of the samples with high correlation with *ASCL1* expression (confirmed in the "2 Variable Analyses"). *SEZ6*, another ASCL1 target gene and an emerging cell surface target for Antibody Drug Conjugates is also highly correlated with both *ASCL1* and *DLL3* expression (Figure 2B). Of note, *SEZ6* expression is highly correlated with *SEZ6L* (SEZ6 homolog like) despite different chromosome locations (17q11.2 and 22q12.1, respectively), suggesting that both genes function in the ASCL1 pathways.

Transcriptome analysis of the NEUROD1 genomic network (Figure 2C) shows that *NEUROD1* expression only accounts for a fraction of the NE samples. Indeed, many samples show high *INSM1* expression without high *NEUROD1* (Figure 2C, compare the 1st and 2nd rows). *NKX2-2* [NK2 transcription factor related, locus 2 (Drosophila)], which is involved in the morphogenesis of the central nervous system (CNS) and a known regulator of NEUROD1 in pancreatic islet cells together with the Neurogenin genes (*NEUROG1* and *NEUROG3*) [12] are co-expressed with *NEUROD1* (Figure 2C). The coexpression of *PAX6* (Paired Box Homeotic Gene-6) encoding a transcription factor for the development of the eyes, nose, pancreas and CNS, is logical as PAX6 controls *NEUROD1* expression [13]. Using the "2 variable Analysis" and the "Compare Patterns" tools of SCLC TumorMiner (see Figure 1A), we discovered coexpression of two genes encoding cell surface proteins and potential targets for immune therapies, *GFRA1* (Glial Cell Line-Derived Neurotrophic Factor Receptor Alpha) and *SEMA6A* (encoding one of the semaphorin) [14] (Figure 2C). Like the samples from untreated patients, the SCLC cell lines also express significant levels of *SEMA6A* with high correlation with *NEUROD1* ($p = 0.57$ with p-value = 2.7e-11) [4]. Whether NEUROD1 directly drives *GFRA1* and *SEMA6A* expression remains to be determined.

The POU2F3 network shows the expected inverse expression between *POU2F3* and *INSM1* (Figure 2D, compare the 1st and 2nd rows) as the POU2F3 cells are derived from the Tuft cells of the bronchial epithelium and are non-NE [15-17]. Figure 2D shows that the tumor samples expressing *POU2F3* coexpress 4 transcription factors known to drive *POU2F3* expression [15,18]: *ASCL2, COLCA2* (also known as *OCAT-2* or *POU2AF3*), *C11orf53* (also known as *OCAT-1* or *POU2AF2*) and *SOX9*. *POU2F3* is also highly correlated with the Tuft-ionocyte progenitor specific genes *FOXI1* and *AVIL* [16,17], as well as with *TRPM5* (Transient Receptor Potential Cation Channel Subfamily M Member 5), which encodes a cell surface ion channel protein highly expressed in bronchial Tuft cells and involved in immune defense [19]. This suggests that TRPM5 could be considered as cell surface target for SCLC-P tumors. Figure 2D also shows that the POU2F3 network/pathway is coordinated with the Notch pathways, as *POU2F3* expression is highly correlated with *REST* and its transcriptional activator *NOTCH1* (validated in the "2 variable analysis" for the untreated samples). *MYC* expression is also highly correlated with *POU2F3*, consistent with independent reports [9,17,20]. These findings suggest that the expression of the 11 genes displayed in Figure 2D could be used as predictors for POU2F3 expression in tumor samples (Figure S2C) and for classifying a given tumor sample as SCLC-P.

Analysis of the YAP1 network across our 3 datasets shows that samples with high *YAP1* expression tend to lack *INSM1* expression (Figure 2E). By contrast, TAZ (encoded by *WWTR1*), the transcriptional co-activator partner of YAP1 is coexpressed with *YAP1*, consistent with the SCLC cell lines (Figure 5 in [4]). Similarly, *TEAD2* and *TEAD3*, the downstream transcription factors of YAP/TAZ are coexpressed with *YAP1*, as well as YAP1's transcriptional targets

212 *SMAD6*, *VGLL4* and *PTPN141* [4]. Figure 2 also shows that the cell adhesion genes *CCN1*, *CTNNA1*
213 and *CTNNA2* are coexpressed with *YAP1*. Consistent with the SCLC cell line data (see Figure 5C-
214 D in [4]), Notch pathway activation (*REST*, *NOTCH1* and *NOTCH2*) is associated with the SCLC-
215 Y samples. Together the expression of the 12 genes displayed in Figure 2E significantly predicts
216 *YAP1* expression both in the SCLC tumors and cell lines (Figure S2C) and therefore could be used
217 to classify a given tumor sample as SCLC-Y (Figure S2D).

218 Using *REST* expression as a reporter for the Notch pathway (Figure 2F), we found
219 coexpression of *REST* with the 4 Notch receptors, *NOTCH1-4* and with YAP/TAZ, consistent
220 activation of the Notch pathway by YAP1-mediated transcription [21]. By contrast, expression of the
221 Notch ligands (*JAG1/2*, *DLL3*, *DLL1*, *DLL4* and *DLK1*) is significantly suppressed in the Notch
222 receptor-positive samples and coexpressed with *DLL3* and *ASCL1* (Figure 2F). These findings
223 support the conclusion that the YAP/Notch/REST network controls the NE fate of SCLC cells [21]
224 and vice-versa as DLL3 suppresses Notch signaling in SCLC [22].

225 Figure 2G shows MYC pathway activation in 52% of the untreated patient samples where
226 *MYCL* dominates (36.4% of the samples). *MYCL* expression also appears linked with *ASCL1*
227 expression (SCLC-A) (Figure 2B). By contrast, *MYC* is only highly expressed in a relatively small
228 fraction of the untreated patient samples (15.6%) and primarily in the SCLC-P samples (Figures
229 2D) [23]. Consistent with the fact that *POU2F3* disappears in the relapse samples and that *ASCL1*
230 expression is also attenuated in those samples, the expression of both *MYCL* and *MYC* appears
231 markedly reduced in the samples of patients at relapse (Figure 2G).

232 The conservation of each of the 5 networks described above between tumor samples and
233 cell lines (Figure S2C) implies their predictive value as genomic signatures for tumors driven by
234 ASCL1, NEUROD1, POU2F3, YAP1 and Notch.

235

236 **NAPY classification of SCLC tumors**

237 To identify highly expressed genes, we first analyzed the gene expression distribution for all genes
238 across the datasets (Figure S1B). The 90-percentile expression value cutoff selected
239 log2(FPKM+1) values > 4 for both the untreated and relapse samples. To further increase
240 stringency, we set up a threshold value log2(FPKM+1) > 5 for high gene expression (red lines in
241 Figures 1A and S1A-C, and shaded areas in Figure S1B-C). We also compared the expression of
242 canonical housekeeping genes in the untreated and relapse datasets and found their expression
243 well-above the threshold of 5 and relatively comparable between the untreated and relapse
244 datasets, suggesting limited batch effect (Figure S1C).

245 Using RNA-seq expression levels >5 [log2(FPKM+1)], we could unambiguously assign
246 all the samples from the untreated patients to the NAPY classification (Figures 1B). However, less
247 than half (44%) of the samples from relapse NCI patients could be classified with 22% as high
248 *YAP1* (Figure 1B). This is notably higher than for the untreated patients (22% vs. 2% *YAP1* high;
249 Figure 1B). Notably, based on the same cut-off [log2(FPKM+1)>5], the SCLC cell lines could be
250 classified like the untreated samples, which is consistent with the fact that most SCLC cell lines
251 have been derived from patients before treatment [24,25].

252 To classify the samples from relapse patients, we first attempted to extend the gene list for
253 cluster analyses by adding to the 4 NAPY genes (highlighted in red in Figure 3A-B), the two NE
254 genes (*INSM1* and *CHGA*), *MYC*, *REST,* and 4 innate immune genes of the major

histocompatibility complex (MHC): *HLA-A*, *HLA-B*, *HLA-C* and *B2M* as reporters of an inflamed signature (SCLC-I) [5]. This 12-gene algorithm classified the samples of untreated patients in 2 groups (Figure 3A; see annotations under the heatmap): SCLC-NE (≈ 70% of the samples) and SCLC-P with high *POU2F3*, *MYC*, *REST* and to a lesser extent *YAP1 e*xpression. The inflamed group with high MHC expression (*HLA-A/B/C* and *B2M*) was found diffuse (≈ 50% of the patient samples) with tendency to be excluded from the SCLC-NE group. For the samples of relapsed patients, the 12 gene signature only clustered the samples based on the MHC genes (≈ 50% of the samples; SCLC-I) (Figure 3B). To overcome the difficulty of classifying the samples from patients at relapse using the NAPY classification, we performed NMF (Non-Negative Matrix Factorization) analyses [5].

NMF classification of SCLC tumors

To perform these NMF analyses, we used the top 5000 most variably expressed protein-coding genes separately in the untreated (UoC and TU) and relapse (NCI) datasets (Figure 3C, Tables S3 and S4). Among those genes, 64.4% are common for the untreated and relapse samples (Figure S4A). Cophenetic and Silhouette scores showed that 4 clusters gave a satisfactory division of the samples (Figure S4B-C).

To develop open-access NMF signatures, we first took the genes with a 2-fold selectivity compared to the genes in the other 3 NMF groups. This led to a list of genes in each NMF group. For the relapse samples, we selected 181 genes for NMF1r, 58 for NMF2r, 342 for NMF3r and 215 for NMF4r (Table S5). For the untreated samples, we obtained 54 genes for NMF1u, 137 for NMF2u, 85 for NMF3u and 386 for NMF4u (Table S6). At the end, we obtained 662 and 795 genes for the untreated and relapse cohorts, respectively (see Method section for details). The top-30 genes for each of the NMFu and NMFr clusters are displayed in Figure 3D and Figure 3E, respectively. Notably, only a few genes are common in the NMF clusters of untreated and relapse patient samples (see diagonal lines between panels D and E in Figure 3 and see Tables S5 and S6).

Pathway analysis shows that NMF1u consists of genes involved in translation and RNA metabolism (Figure 4A) in addition to *ASCL1* (Figures 3D, F, H)). The NE enrichment of NMF1u is easily visible through the mapping *ASCL1*, *NEUROD1*, *INSM1* and *CHGA* in the NMFu clusters (Figure 3F). NMF2u also shows strong NE enrichment (Figures 3F and 4A) and includes *NEUROD1* (Figure 3D). NMF3u includes *POU2F3* (Figures 3F and 3H) and immune and interleukin pathways (Figure 4A) as well as the MYC pathway (Figures 3D; *MYC* and *MYB* annotated in red). NMF4u partially extends to NMF3u and shows positive enrichment for immune, cytokine and interferon pathways (Figures 3D and 4A). It is enriched for *YAP1* (Figures 3F & H).

Pathway analyses for the 4 relapse NMF clusters shows that NMF1r includes genes and pathways related to NE differentiation (Figures 4B and 3E) as well as *ASCL1* (Figures 3G-H). NMF2r comprises NEUROD1 (Figure 3E and 3H) and is enriched for cell cycle genes (Figure 4B). NMF3r includes genes involved in metabolism and complement (Figure 4B). It also includes *YAP1* (Figure 3G-H). NMF4r consists specifically of immune genes (Figures 3E and 4B) and some *YAP1*-expressing samples (Figures 3G and 3H). The complete pathway enrichment results for untreated and relapse SCLC samples are provided in Table S7 and Table S8, respectively.

The NMF clusters reflect the SCLC TumorMiner molecular signatures

298 Next, we explored the correlations between the NMF and eight transcriptional signatures provided
299 in SCLC TumorMiner: NE (Neuroendocrine), RepStress (Replication stress), CES (Chromosome
300 Centromere and Kinetochore score), Epithelial, Stroma, Immune, APM (Antigen Presenting
301 Machinery) and Ychrom (Y-chromosome), which were computed as the mean expression of the
302 genes included in each signature (see Methods section).

303 Figure 4C tabulates the Pearson coefficient correlations between each NMF and the 8
304 signatures with the colors reflecting the direction and intensity of the correlations (red for positive
305 and blue for negative). Consistent with the top gene signatures and the Reactome pathway analyses
306 (see Figure 4A-B), the NMF1u, NMF2u, NMF1r and NMF2r signatures are highly correlated with
307 the NE signature as well as with the RepStress and CES signatures. They are also significantly
308 devoid of the Immune, APM and Stroma signatures (Figure 4C). Conversely, NMF3u, NMF3r,
309 NMF4u and NMF4r are enriched for the Immune, APM, Stroma and epithelial signatures and lack
310 the NE, RepStress and CES signatures. Together these results demonstrate the functional
311 significance of the NMF classifications for SCLC.

312

313 **External validation of the NMFs**

314 To evaluate and validate our NMF-based gene signatures using independent datasets, while
315 avoiding batch effect correction with the training data, we computed NMF scores for each sample
316 based on the signature genes. We then clustered samples using the top 30 most differentially
317 enriched genes and assessed whether the resulting patterns were consistent with those observed in
318 the training datasets. We first performed validation using RNA-seq data from two external
319 untreated SCLC cohorts, GSE60052 [26] (n = 79) and IMpower133 [8] (n = 271). As both cohorts
320 consist of treatment-naïve samples, we applied the NMFu untreated signatures for clustering and
321 validation (Table S6). As shown in Supplementary Figure S5A-B, the top 30 most differentially
322 enriched genes were consistent with those identified in our untreated training SCLC cohort.
323 Neuroendocrine (NE) markers, including ASCL1, NEUROD1, INSM1 and CHGA, as well as non-
324 NE markers such as POU2F3, YAP1, MYC and REST, exhibited distinct and consistent
325 enrichment patterns across clusters in both external cohorts. These findings support the biological
326 relevance and reproducibility by identifying the same 4 NMF signatures for untreated samples in
327 these two other external datasets.

328 Next, we sought to validate the NMF relapse signature using the Wagner dataset [27], which
329 includes 22 samples from 18 relapse SCLC patients. As this dataset contains two technical batches
330 (RNA-seq protocols: polyA and total RNA; both derived from frozen samples), we applied batch
331 correction as described in the original study. As shown in Figure S6A, the top 30 most
332 differentially enriched genes were consistent with those observed in three of our relapse SCLC
333 clusters: NMF1r, NMF2r and NMF4r. We did not identify a cluster corresponding to NMF3r of
334 the NCI training dataset, which is associated with complement and metabolic pathways. To further
335 investigate the consistency of the 4 NMF relapsed clusters, we applied the NMF method on the
336 Wagner dataset using the same set of input genes (~5000 genes) (as with the NCI dataset) and
337 computed the correlation between the metagenes from the NCI basis matrix to the equivalent
338 matrix generated for the Wagner dataset. Figure S6C shows the correlation of Wagner metagene
339 groups with the NCI metagene groups. Wagner W3 group only had low correlation to the NCI
340 groups (r=0.29), whereas other subgroups had correlations greater than 0.6 (for W1, W2 and W4).
341 This discrepancy may be due to differences in sample composition, including the absence of liver

342 metastasis samples and variation in biopsy sites between the NCI and Wagner datasets (see Figure
343 S6B).

344

345 **Prognosis biomarkers and risk factors**

346 SCLC TumorMiner is designed to assess prognosis biomarkers associated with gene expression,
347 mutations, clinical metadata and NMF signatures. The default display on the website is for *SLFN11*
348 (Figure 5A). *SLFN11*'s wide range of expression in SCLC samples (Figures 6E-F) and SCLC cell
349 lines [4] as well as its predictive value to predict response to chemotherapeutic agents targeting DNA
350 replication [28,29] (see next section) qualifies it as a quantitative biomarker. Figure 5A shows that
351 high *SLFN11* expression in the untreated TU dataset is associated with improved survival. This
352 observation agrees with a recent publication demonstrating preferential response of SLFN11-
353 expressing cells to the DNA-targeted chemotherapies used to treat SCLC [30].

354 SCLC TumorMiner also allows multivariable analyses by combining different genes or
355 signatures. Figure 5B-C shows the predictive value of combining the expression of *SEZ6*, *SRSF1*
356 (encoding the Serine and Arginine Rich Splicing Factor 1) [26] with the proliferation marker *MKI67*
357 in the 150 untreated patients (HR 2 groups = 1.7; p-value = 0.016). In the multivariable Cox
358 analysis, age, sex, and SEZ6 expression were independent predictors of survival, with older age,
359 male sex, and high SEZ6 associated with increased hazard. SLFN11 showed a borderline
360 protective effect, while tumor stage and other genes (MKI67 and SRFS1) were not significant after
361 adjustment. These results suggest that SEZ6 provides prognostic value beyond conventional
362 clinical factors and may improve risk stratification. Additional predictive biomarkers can be
363 searched using the Lasso analysis option (highlighted in yellow at the bottom left in Figure 5A).

364 The prognostic value of each of the eight NMF gene signatures can also be explored in the
365 "Prognosis Biomarkers" tool of SCLC TumorMiner. Figure 5D shows that at diagnosis before
366 treatment, patients classified as NMF1u appear to have a better prognosis than patients in the
367 MMF2u subgroup. This appears different for patients at relapse, where the NMF3r group appears
368 at higher risk (Figure 5D).

369 The prognostic value of each of the eight gene signatures can also be explored in SCLC
370 TumorMiner. Figure 5E shows the good prognosis value of the APM, immune, and Stroma
371 signatures while male patients tend to have poor survival in the untreated datasets. This observation
372 further indicates that tumors with high immune and stroma infiltration respond better to treatments.

373 None of the NAPY genes show significant predictive value, even in the untreated patients
374 despite their broad differential expression (see Figure 1). Similarly, *MYC*, *MYCL*, *REST* and
375 *NOTCH* do not show significant predictive value. On the other hand, consistent with a recent study
376 reporting that high expression of *SRSF1* is linked with poor survival in SCLC patients [26], we
377 observe that high expression of *SRSF1* is a risk factor for the untreated patients (Figure 5F). Single
378 gene analyses also confirm the poor prognostic value of *SEZ6* in the untreated patient datasets and
379 the good prognostic value of high *SFLN11* expression in the patients at relapse (Figure 5F).

380

381 **Predictive biomarkers for cell surface targets**

382 Thirteen Antibody Drug Conjugates (ADCs) have been approved by the FDA in the past 6 years.
383 Datroway® (Datopotamab Deruxtecan), the most recent (January 2025) delivers the TOP1

384 inhibitor Deruxtecan to triple-negative breast cancers (TNBC) expressing TROP2 (encoded by
385 *TACSTD2*). Notably the other TROP2-targeted TOP1 ADC, Trodelvy® (Sacituzumab Govitecan)
386 has been granted Breakthrough Therapy Designation for ES-SCLC patients [31]. CAR-T cells and
387 bi- and tri-specific T-cell engagers are also in active development with the recent approval of the
388 T-cell engager Imdelltra® (Tarlatamab-dlle) for ES-SCLC [32]. However, DLL3 or TROP2 are not
389 validated companion diagnostic (CDx) for patient selection and, to our knowledge, RNA-seq has
390 not been fully explored in clinical trial analyses.

391 Figures 6A-B display the expression of selected clinically relevant cell surface target genes
392 (Table S9). As shown in Figures 6A and C, *DLL3* shows a broad range of expression in the
393 untreated patient samples with the highest levels in the NE samples matching the NMF1u &
394 NMF2u groups (Figure 6C). Notably, in the samples of patients at relapse, DLL3 expression is at
395 least 3-fold lower and lacks clear discrimination among the NMFs groups (compare Figures 6C
396 and D), consistent with the reduced *ASCL1* expression at relapse (see Figure 1A). These results
397 suggest the potential of measuring *DLL3* transcripts as a CDx in front-line SCLC.

398 TROP2 (encoded by *TACSTD2*) appears generally low at relapse (Figure 6B) while, in the
399 untreated patients, its expression is high in samples with low NE score and high APM score (Figure
400 6A). Accordingly, TROP2 expression matches the NMF3u (*POU2F3*-endriched) and NMF4u
401 (Immune-enriched) clusters (Figure 6).

402 Figure 6 (upper panels A-D) displays the expression of additional cell surface targets for
403 ADCs that are in clinical trials (Table S9). *DLK1* (Delta Like Non-Canonical Notch Ligand 1) is
404 highly expressed untreated samples with NE signature (Figure 6A) and less in relapse tumors
405 (Figure 6A-D). NMF analyses show high *DLK1* expression in the NMF1u and NMF2u and in
406 approximately 50% of the NMF4u group (Inflammatory and Immune) (Figure 6C). These results
407 support the ongoing clinical trial testing a DLK1-ADC in NE tumors [33].

408 Two of the carcinogenic embryonic antigens (encoded by *CEACAM5* and *CEACAM6*),
409 which are targeted with ADCs in clinical trials for colon, gastric cancers and NSCLC (Table S9),
410 are highly expressed in the samples classified as NMF1u and NMF2r (Figures 6A-D). These results
411 suggest the potential of CEACAM5/6-targeted ADCs in SCLC and the potential of measuring
412 CEA in the blood of SCLC patients as a CDx biomarker [34,35].

413 *CLDN18* (coding for Claudin 18), an ADC target for pancreatic cancer (Table S9) is highly
414 expressed in a few untreated patients; yet, not in relapse patients (Figures 6A-B). As discussed
415 above, *SEZ6*, a downstream target of ASCL1 [36] is highly expressed across untreated and relapse
416 samples matching the NE signature with only partial overlap with *DLL3* expression (Figures 6A-
417 D). Finally, B7H3 (encoded by *CD276* and belonging to the immunoglobulin superfamily) is
418 expressed in a broad range of samples (Figures 6A-D). Together, these results validate the potential
419 of DLL3-, SEZ6-, DLK1-, CEACAM-, CLDN18 and B7H3-targeted ADCs in SCLC [37].

420

421 **Predictive pharmacodynamic (PD) biomarkers related to the ADC payloads**

422 The bottom panels of Figures 6 summarize the expression of known intracellular drug targets
423 (Figure 6E-F), drug efflux transporters (Figure 6G-H) and proapoptotic genes (Figure 6I-J).

424 *SLFN11* (Schlafen 11) shows a broad expression range (over 8-fold) in both the untreated
425 and relapse patient samples, in agreement with SLFN11's wide distribution across the SCLC cell
426 lines irrespective of the NAPY subgroups [4] (https://discover.nci.nih.gov/SclcCellMinerCDB/).

427 Consistent with *SLFN11* being an immune- and interferon-response gene [28], the NMF4
428 inflammatory/immune subgroups tend to show highest *SLFN11* expression both in the untreated
429 and relapse patient samples (Figure 6E and F). The broad range of SLFN11 expression suggests
430 that further studies are warranted to confirm the relevance of SLFN11 to predict response of
431 patients treated with lurbinectedin, topotecan and TOP1 inhibitor payload ADCs [38-42].

432 Since TOP1 is the primary cellular target of topotecan, irinotecan and TOP1-ADCs, and
433 TOP2 the target of etoposide, we looked at *TOP1* and *TOP2* expression (Figure 6E-F). Both are
434 highly expressed in the samples from untreated and relapse patients as expected for housekeeping
435 genes. Thus, *TOP1* and *TOP2* levels are irrelevant as predictive biomarkers.

436 Lack of O-6-Methylguanine-DNA Methyl-Transferase (MGMT) predicts the activity of
437 DNA alkylating agents, and foremost of temozolomide [43], which is occasionally used in SCLC [44].
438 Figure 6 (right panels E & F) shows low expression MGMT in some samples, suggesting the
439 potential of testing *MGMT* expression for temozolomide treatments.

440 Drug efflux transporters of the ABC family are a major cause of resistance to tubulin
441 inhibitors (vinca and auristatin derivatives) that are commonly used as ADC payloads. Yet,
442 measuring ABC transporters is not done in clinical routine. Figure 6G-H displays the expression
443 of the main ABC transporter genes. *ABCB1*, which encodes P-glycoprotein (PgP) has notably low
444 expression both in the untreated and relapse samples, while *ABCC2* and *ABCC3* show significant
445 overexpression in the NMF3r cluster (Figure 6H). These results suggest that measuring ABC
446 transporters should be considered for ADCs with anti-tubulin payloads.

447 Because broad resistance to chemotherapy is dependent on reduced apoptosis, we explored
448 apoptotic genes. Figures 6I-J and S9C show global suppression of proapoptotic gene expression
449 in relapse patient, which may account, in part for the overall resistance of relapse patients to
450 chemotherapy.

451

452 **Analysis of individual patients using the "MyPatient" tab of SCLC TumorMiner**

453 Going forward, we wish to propose SCLC TumorMiner as a prototype clinical interface for
454 classifying tumors and for predicting risk factors and rational therapies (Figure 7A). This feature
455 is included in the "My patient" tab of SCLC TumorMiner (Annotation #7 at the top of Figure 1A).

456 As discussed above (see Figure 1B), all the untreated patient samples can be assigned to at
457 least one of the NAPY groups based on the high expression cut-off of log2(FPKM+1) > 5 defined
458 above. Therefore, we have included the NAPY classification to effectively characterize the
459 samples from untreated patients in the "My patient" tab of SCLC TumorMiner. The situation is
460 different for the relapse SCLC samples. Indeed, based on the expression cut-off of log2(FPKM+1)
461 > 5, less than half of the samples (44%) can be assigned to the NAPY groups, with the YAP1
462 group (SCLC-Y) being prominent (22%) (see Figure 1B).

463 Faced with the limitation of the NAPY classification for the relapse patient samples and
464 the positive discriminatory value of the NMF classification (see Figures 3 and S4), we developed
465 an algorithm to classify the relapse samples based on NMF. Figure S7 shows the average
466 expression scores for the NMFr clusters of the 50 samples from the NCI relapse patients. Based
467 on this plot, we chose a threshold of 4 to assign samples to each NMFr cluster. This approach
468 enables the computation of mean average NMF scores for individual samples. On the website, we
469 implemented this approach to score automatically individual samples in the "MyPatient" tab of

470 SCLC TumorMiner. Upon typing a patient identifier (code) (Figure 7B), SCLC-TumorMiner
471 displays both NAPY and NMF classifiers for cataloging individual patient samples (Figure 7B-C).

472 The tab "My Patient" also displays predictive biomarkers for therapies (Figure 7B-C). This
473 is done by the TumorMiner software, which queries a dataset listing 63 cell surface targets for
474 ADCs currently FDA-approved and in clinical development (Table S9). Our website displays the
475 cell surface targets expressed above a threshold of 6 (log2(FPKM+1)). For example, in Figure 7C,
476 the displayed patient tumor sample overexpresses NCAM1 and FN1 implying that the patient
477 could be candidate for ADCs comprising NCAM1 or FN1 antibodies.

478 These results highlight the translational potential of the SCLC TumorMiner platform for
479 individualized patient care. While traditional NAPY classification remains useful for untreated
480 tumors, its limited applicability to relapsed samples underscores the importance of alternative
481 classifiers. By implementing NMF-based transcriptomic classifiers and integrating biomarker-
482 based predictions for targeted therapies, the "MyPatient" module can provide real-time,
483 personalized tumor profiling. Our goal is to facilitate not only tumor subtype identification but
484 also actionable therapeutics, bridging molecular characterization with clinical decision-making in
485 SCLC. As the platform evolves with more comprehensive datasets, it holds promise for guiding
486 precision medicine strategies in both newly diagnosed and treatment-refractory patients.

487

488 **DISCUSSION**

489 Mining cancer patient clinical and genomics data is critical for understanding a disease,
490 discovering biomarkers, predicting outcomes, optimizing treatments, and ultimately shifting
491 patient care to a logic-based and flexible paradigm. During the last decade, new tools have emerged
492 such as cBioPortal (http://cbioportal.org) [45] or Xena (https://xena.ucsc.edu) [46] , GEPIA2
493 (http://gepia.cancer-pku.cn/) [47], UALCAN (https://ualcan.path.uab.edu/) [48] or Survsig
494 (https://survsig.hcemm.eu/), offering different functions for genomic data visualization and
495 analyses.

496 Here we introduce "SCLC TumorMiner", a web application for SCLC patient genomics.
497 Its architecture and displays are constructed like SCLC-CellMinerCDB
498 (https://discover.nci.nih.gov/SclcCellMinerCDB), which enables users to compare tumor samples
499 with a broad collection of SCLC cell lines [4,49]. SCLC TumorMiner complements existing tools for
500 mining SCLC patient clinical and genomics information, such as cBioPortal, Xena or Survsig. It
501 is also meant to improve access and interpretation for physicians and their patients. SCLC
502 TumorMiner has its own specific datasets and unique functionalities to build predictive models
503 and generate prognostic gene sets. It is the first tool to enable comparison between a patient sample
504 and other patient samples or cell lines. Table S10 showcases the distinctive values of SCLC
505 TumorMiner with other tools.

506 SCLC TumorMiner (https://discover.nci.nih.gov/SclcTumorMinerCDB/) has a battery of
507 unique tools (see Figure 1A) allowing real-time display of omics data for individual genes and
508 individual patient samples (*2-Variable Analyses*, *Prognosis Biomarkers* and *Predictive*
509 *Biomarkers*) or for multiple genes to explore molecular networks (*Multivariable Analyses* and
510 *Compare Patterns* tools) (see Figure 1A). It integrates 8 pathway *Signatures* relevant to SCLC
511 biology (NE, RepStress, CES, APM, Immune, EMT, Stroma, Y-Chrom), 50 Hallmark signatures
512 and 63 cell surface targets relevant to the current development of Antibody Drug Conjugates

513 (ADCs), Bispecific T-cell engagers (BiTEs) and CAR-T cell therapies. Data can be downloaded
514 from the SCLC TumorMiner website for further analyses, as demonstrated in this report by the
515 different plots comparing gene expression in untreated and treated patients and in samples from
516 different NMF groups.

517 A biologically relevant feature of TumorMiner is its ability to explore the logic of
518 molecular networks/pathways based on the premise that individual components of molecular
519 pathways are quantitatively linked and significantly correlated [4]. Figures 2 and S2 demonstrate
520 that each of the NAPY genes has its own network (genomic identity) across tumor samples and
521 that these networks are highly conserved across patient samples and cell line models (Figure S2C),
522 implying their robustness. A notable finding is the interconnection between the Notch, the
523 YAP/TAZ and the ASCL1-NE pathways whereby expression of the YAP/TAZ pathway is tightly
524 linked to activation of the Notch pathway; and vice-versa that activation of the NE (ASCL1-SEZ6)
525 pathway is associated with expression of the Notch ligands (DLL3, DLK1, DLL1, DLL4 and
526 JAG2) and negatively correlated with the Notch receptors and their transcription effector REST
527 (see Figure 2F). These results suggest feedback loops involving the non-NE pathways including
528 YAP/TAZ and the Notch receptors, and the NE pathway including ASCL1 and the Notch ligands
529 [21,22]. Whether and how YAP/TAZ functions upstream of the Notch transcription factor REST
530 remains to be established.

531 Cancer cell plasticity and heterogeneity are two outstanding characteristics of SCLC [50-56].
532 This is exemplified by the fact that at relapse, patients become resistant to chemotherapy after
533 initially responding generally dramatically. Accordingly, SCLC TumorMiner reveals key genomic
534 differences between the samples of untreated and relapsing patients. One such difference is the
535 loss of the bimodal expression of NEUROD1, ASCL1 and POU2F3 and the upregulation of YAP1
536 at relapse (see Figure 1). This could have, at least two not mutually exclusive explanations: 1/
537 differentiated cancer cells expressing ASCL1 (NE cells) or POU2F3 (Tuft-ionocyte-like cells) are
538 eliminated by the 1st line of chemotherapy (see Figures 1A and S1B), leaving behind less
539 differentiated resistant cells; 2/ chemotherapy is less effective toward the less differentiated and
540 more plastic tumor cells with basal cell characteristics [55], which remain in the tumor and become
541 prominent at relapse.

542 Another notable difference between untreated tumors and tumors at relapse is the
543 significant downregulation of MYCL at relapse (see Figure 2G). This reduction is likely
544 consequential to the fact that ASCL1 is a transcriptional driver of MYCL [57] (as visualized in
545 Figures 2B) [57] and that ASCL1 expression is significantly suppressed in relapsed tumors (see
546 Figures 1A and B).

547 With respect to the chemoresistance of relapsed tumors, it is likely multifactorial. Indeed,
548 while the expression of SLFN11 and some of the proapoptotic genes (BAD, BAX, BID, NOXA
549 and PUMA) is high in chemotherapy-naïve patient samples, it is markedly reduced in relapsed
550 tumors (see Figures 6), suggesting that the initial response of patients to various chemotherapies
551 is driven, in part by pro-apoptotic genes and SLFN11. Conversely, resistance may involve
552 downregulation of SLNF11 and the cell death pathways. Whether these pathways are
553 epigenetically suppressed in relapse tumors and could be reactivated by HDAC and EZH2
554 inhibitors remains to be tested [10,39,58].

555 Bispecific antibodies T-cell engagers (BiTEs), antibody drug conjugates (ADCs), and
556 CAR-T are in full development. Regarding the therapies targeting DLL3, Tarlatamab (Imdelltra®)

557 and Zocilurtatug Pelitecan (Zl-1310) (NCT06179069), expression of DLL3 is generally lower at
558 relapse than in untreated patients, consistent with DLL3 being a direct transcriptional target of
559 ASCL1, which is significantly suppressed at relapse (Figures 6 & S9) [4,57]. This may justify moving
560 Tarlatamab and Z-1310 to 1st line therapy. Also, since DLL3 IHC analyses have until now failed
561 to predict responses [59], using RNAseq could identify responders (approximately 40%) to
562 Tarlatamab [32,59] and Z-1310 (NCT06179069), thereby avoiding unnecessary toxicity and cost.
563 Surprisingly, expression of TROP2 (encoded by *TACSTD2*) is generally low both in the untreated
564 and relapse patient samples. This questions the potential of Trodelvy® (Sacituzumab Govitecan)
565 or Datroway® (Datopotamab deruxtecan) in SCLC patients irrespective of their disease stage.

566 Based on our observations, SEZ6 appears promising for two of the ADCs in clinical
567 development: ABBV-011 and ABBV-706 (see Table S9). Yet, like DLL3, SEZ6 is a downstream
568 transcriptional target of ASCL1 [36,37] (see Figure 2) and is therefore likely to be more effectively
569 targeted in untreated patients. By contrast, B7H3 (encoded by *CD276*), the target of two ADCs in
570 advanced clinical trial for ES-SCLC: Risvutatug Rezetecan (GSK5764227) and Ifinatamab
571 Deruxtecan (DS-7300) (Table S9) appears highly expressed in a significant fraction of samples
572 from relapsed patients in SCLC TumorMiner. Our systematic screening for other cell surface
573 targets reveals that CEA (carcinoembryonic antigen), which is encoded by *CEACAM5* and
574 *CEACAM6*, is highly expressed in multiple samples from relapse patients (Figure 6), suggesting
575 the potential of CEA-ADCs [60-62]. An advantage of targeting CEA is that, in addition to measuring
576 CEACAAM5/6 transcripts and by IHC in tumor samples, clinical trials could include CEA blood
577 samples [63,64]. We also found that TRPM5, which encodes a sodium channel transporter, is
578 selectively expressed in the POU2F3-expressing tumors and that GFRA1 (Glial Cell Line-Derived
579 Neurotrophic Factor Receptor Alpha) and SEMA6A (encoding one of the semaphorins) [14] are
580 specifically expressed in NEUROD1 expressing SCLC (Figure 2), suggesting they might be
581 considered as novel cell surface targets for SCLC. These analyses demonstrate the potential use of
582 SCLC TumorMiner for discovering novel cell surface therapeutic targets for ADCs, T-Cell
583 Engagers (BiTEs) and CAR-T.

584 As we move toward precision medicine, multivariable analyses will be needed. For
585 instance, for a given cell surface target, clinicians may have to choose between an ADC with a
586 TOP1 or a tubulin payload or a T-cell engager (BiTE). To illustrate this point, one could propose
587 guiding payload choice with at least two biomarkers: SLFN11 and ABC drug efflux transporters.
588 If the tumor expresses high SLFN11 and drug efflux transporters, TOP1 inhibitors will likely be
589 superior to a tubulin inhibitor ADC, and conversely a tubulin inhibitor ADC payload would be
590 logical for tumors with low SLFN11 and ABC transporters expression. For immune checkpoint
591 inhibitors and BiTEs, one could consider testing the predictive value of high APM and Immune
592 signatures, which would reflect the presence of immune cells in the tumor, or tumor intrinsic
593 features such as high APM or NOTCH1 expression [65,66].

594 Ultimately, we speculate that "*MyPatient*" could be developed for clinical practice as bulk
595 RNA-seq and DNA-seq can routinely be performed. Sequencing results and clinical parameters
596 could be loaded into SCLC TumorMiner. Additionally, the Tumor_Miner architecture and
597 interface could be readily expanded to integrate protein expression (proteomics) and epigenetic
598 (DNA methylome) parameters as we have already done in our CellMiner websites
599 (https://discover.nci.nih.gov/). "My_Patient" could provide a medical interface displaying a
600 patient's genomic parameters, dictating which therapy would be most appropriate and predicting

risk-factors. Finally, one could anticipate future integration of natural-language query interfaces or Chatbot to enhance user accessibility.

LIMITATIONS OF THE STUDY

A limitation of the current study is the technical and clinical heterogeneity of the cohorts. RNA-seq data were generated from both fresh frozen and FFPE samples, with untreated cohorts primarily derived from frozen tissues and the relapse NCI cohort including both frozen and FFPE samples. Analysis of the NCI samples, including 8 frozen biopsy samples and 42 FFPE samples, shows that preservation methods only explain 2.9% of the variance, which is quite low, especially compared to the biopsy site, which explains 10.8% of the variance. Hierarchical clustering analysis of the 204 samples from the 3 datasets (UoC, TU and NCI) also shows a clear separation between NCI (relapse) and the other samples (Untreated). The NCI relapse samples are mostly FFPE, whereas the untreated samples are all Frozen. We cannot remove the effect of the preservation because it is confounded with sample type (relapse vs. untreated). Thus, no batch effect was applied for all 3 datasets, and we believe that bulk RNA-seq of patient samples can give a valuable estimate of gene expression for highly expressed genes [log2(FPKM+1) > 5]. Adding more samples will increase the statistical power and robustness of SCLC TumorMiner. However, a challenge for cross-database analyses is to access large and well-annotated datasets. Material transfer agreements commonly restrict the sharing of FASTQ files and associated clinical data across institutions. **“**MyPatient” module only provides a prototype, and users will have the option to integrate our TumorMiner platform into Electronic Medical Record (EMR) systems to provide “real-time” evaluation of tumor Omics for precision medicine.

625 **REFERENCES**
626

627 1. Thomas, A., Takahashi, N., Oplustil O'Connor, L., Redon, C.E., Mohindroo, C., Sciuto,
628 L., Pongor, L., Schmidt, K.T., Steinberg, S.M., Aladjem, M.I., et al. (2025). Tumor-
629 targeted top1 inhibitor delivery with optimized parp inhibition in advanced solid tumors:
630 a phase i trial of gapped scheduling. Nature Communications *16*, 9457. 10.1038/s41467-
631 025-64509-5.
632 2. George, J., Lim, J.S., Jang, S.J., Cun, Y., Ozretic, L., Kong, G., Leenders, F., Lu, X.,
633 Fernandez-Cuesta, L., Bosco, G., et al. (2015). Comprehensive genomic profiles of small
634 cell lung cancer. Nature *524*, 47-53. 10.1038/nature14664.
635 3. Rudin, C.M., Poirier, J.T., Byers, L.A., Dive, C., Dowlati, A., George, J., Heymach, J.V.,
636 Johnson, J.E., Lehman, J.M., MacPherson, D., et al. (2019). Molecular subtypes of small
637 cell lung cancer: a synthesis of human and mouse model data. Nat Rev Cancer.
638 10.1038/s41568-019-0133-9.
639 4. Tlemsani, C., Pongor, L., Elloumi, F., Girard, L., Huffman, K.E., Roper, N., Varma, S.,
640 Luna, A., Rajapakse, V.N., Sebastian, R., et al. (2020). SCLC-CellMiner: A Resource for
641 Small Cell Lung Cancer Cell Line Genomics and Pharmacology Based on Genomic
642 Signatures. Cell Rep *33*, 108296. 10.1016/j.celrep.2020.108296.
643 5. Gay, C.M., Stewart, C.A., Park, E.M., Diao, L., Groves, S.M., Heeke, S., Nabet, B.Y.,
644 Fujimoto, J., Solis, L.M., Lu, W., et al. (2021). Patterns of transcription factor programs
645 and immune pathway activation define four major subtypes of SCLC with distinct
646 therapeutic vulnerabilities. Cancer Cell *39*, 346-360 e347. 10.1016/j.ccell.2020.12.014.
647 6. Pacheco, J., and Bunn, P.A. (2019). Advancements in Small-cell Lung Cancer: The
648 Changing Landscape Following IMpower-133. Clin Lung Cancer *20*, 148-160 e142.
649 10.1016/j.cllc.2018.12.019.
650 7. Paz-Ares, L., Dvorkin, M., Chen, Y., Reinmuth, N., Hotta, K., Trukhin, D., Statsenko, G.,
651 Hochmair, M.J., Ozguroglu, M., Ji, J.H., et al. (2019). Durvalumab plus platinum-
652 etoposide versus platinum-etoposide in first-line treatment of extensive-stage small-cell
653 lung cancer (CASPIAN): a randomised, controlled, open-label, phase 3 trial. Lancet *394*,
654 1929-1939. 10.1016/S0140-6736(19)32222-6.
655 8. Nabet, B.Y., Hamidi, H., Lee, M.C., Banchereau, R., Morris, S., Adler, L., Gayevskiy,
656 V., Elhossiny, A.M., Srivastava, M.K., Patil, N.S., et al. (2024). Immune heterogeneity in
657 small-cell lung cancer and vulnerability to immune checkpoint blockade. Cancer Cell.
658 https://doi.org/10.1016/j.ccell.2024.01.010.
659 9. Liu, Q., Zhang, J., Guo, C., Wang, M., Wang, C., Yan, Y., Sun, L., Wang, D., Zhang, L.,
660 Yu, H., et al. (2024). Proteogenomic characterization of small cell lung cancer identifies
661 biological insights and subtype-specific therapeutic strategies. Cell *187*, 184-203 e128.
662 10.1016/j.cell.2023.12.004.
663 10. Tang, S.W., Thomas, A., Murai, J., Trepel, J.B., Bates, S.E., Rajapakse, V.N., and
664 Pommier, Y. (2018). Overcoming Resistance to DNA-Targeted Agents by Epigenetic
665 Activation of Schlafen 11 (SLFN11) Expression with Class I Histone Deacetylase
666 Inhibitors. Clin Cancer Res *24*, 1944-1953. 10.1158/1078-0432.CCR-17-0443.
667 11. Pozo, K., Kollipara, R.K., Kelenis, D.P., Rodarte, K.E., Ullrich, M.S., Zhang, X., Minna,
668 J.D., and Johnson, J.E. (2021). ASCL1, NKX2-1, and PROX1 co-regulate subtype-
669 specific genes in small-cell lung cancer. iScience *24*, 102953.
670 https://doi.org/10.1016/j.isci.2021.102953.

671 12. Anderson, K.R., Torres, C.A., Solomon, K., Becker, T.C., Newgard, C.B., Wright, C.V.,
672 Hagman, J., and Sussel, L. (2009). Cooperative transcriptional regulation of the essential
673 pancreatic islet gene NeuroD1 (beta2) by Nkx2.2 and neurogenin 3. J Biol Chem *284*,
674 31236-31248. 10.1074/jbc.M109.048694.
675 13. Gosmain, Y., Marthinet, E., Cheyssac, C., Guerardel, A., Mamin, A., Katz, L.S.,
676 Bouzakri, K., and Philippe, J. (2010). Pax6 controls the expression of critical genes
677 involved in pancreatic alpha cell differentiation and function. J Biol Chem *285*, 33381-
678 33393. 10.1074/jbc.M110.147215.
679 14. Mastrantonio, R., You, H., and Tamagnone, L. (2021). Semaphorins as emerging clinical
680 biomarkers and therapeutic targets in cancer. Theranostics *11*, 3262-3277.
681 10.7150/thno.54023.
682 15. Huang, Y.H., Klingbeil, O., He, X.Y., Wu, X.S., Arun, G., Lu, B., Somerville, T.D.D.,
683 Milazzo, J.P., Wilkinson, J.E., Demerdash, O.E., et al. (2018). POU2F3 is a master
684 regulator of a tuft cell-like variant of small cell lung cancer. Genes Dev *32*, 915-928.
685 10.1101/gad.314815.118.
686 16. Montoro, D.T., Haber, A.L., Biton, M., Vinarsky, V., Lin, B., Birket, S.E., Yuan, F.,
687 Chen, S., Leung, H.M., Villoria, J., et al. (2018). A revised airway epithelial hierarchy
688 includes CFTR-expressing ionocytes. Nature *560*, 319-324. 10.1038/s41586-018-0393-7.
689 17. Ireland, A.S., Xie, D.A., Hawgood, S.B., Barbier, M.W., Zuo, L.Y., Hanna, B.E., Lucas-
690 Randolph, S., Tyson, D.R., Witt, B.L., Govindan, R., et al. (2025). Basal cell of origin
691 resolves neuroendocrine-tuft lineage plasticity in cancer. Nature. 10.1038/s41586-025-
692 09503-z.
693 18. Wu, X.S., He, X.Y., Ipsaro, J.J., Huang, Y.H., Preall, J.B., Ng, D., Shue, Y.T., Sage, J.,
694 Egeblad, M., Joshua-Tor, L., and Vakoc, C.R. (2022). OCA-T1 and OCA-T2 are
695 coactivators of POU2F3 in the tuft cell lineage. Nature *607*, 169-175. 10.1038/s41586-
696 022-04842-7.
697 19. Abdel Wadood, N., Hollenhorst, M.I., Elhawy, M.I., Zhao, N., Englisch, C., Evers, S.B.,
698 Sabachvili, M., Maxeiner, S., Wyatt, A., Herr, C., et al. (2025). Tracheal tuft cells release
699 ATP and link innate to adaptive immunity in pneumonia. Nature Communications *16*,
700 584. 10.1038/s41467-025-55936-5.
701 20. Baine, M.K., Febres-Aldana, C.A., Chang, J.C., Jungbluth, A.A., Sethi, S., Antonescu,
702 C.R., Travis, W.D., Hsieh, M.S., Roh, M.S., Homer, R.J., et al. (2022). POU2F3 in
703 SCLC: Clinicopathologic and Genomic Analysis With a Focus on Its Diagnostic Utility
704 in Neuroendocrine-Low SCLC. J Thorac Oncol *17*, 1109-1121.
705 10.1016/j.jtho.2022.06.004.
706 21. Shue, Y.T., Drainas, A.P., Li, N.Y., Pearsall, S.M., Morgan, D., Sinnott-Armstrong, N.,
707 Hipkins, S.Q., Coles, G.L., Lim, J.S., Oro, A.E., et al. (2022). A conserved
708 YAP/Notch/REST network controls the neuroendocrine cell fate in the lungs. Nat
709 Commun *13*, 2690. 10.1038/s41467-022-30416-2.
710 22. Kim, J.W., Ko, J.H., and Sage, J. (2022). DLL3 regulates Notch signaling in small cell
711 lung cancer. iScience *25*, 105603. 10.1016/j.isci.2022.105603.
712 23. Ireland, A.S., Micinski, A.M., Kastner, D.W., Guo, B., Wait, S.J., Spainhower, K.B.,
713 Conley, C.C., Chen, O.S., Guthrie, M.R., Soltero, D., et al. (2020). MYC Drives
714 Temporal Evolution of Small Cell Lung Cancer Subtypes by Reprogramming
715 Neuroendocrine Fate. Cancer Cell *38*, 60-78 e12. 10.1016/j.ccell.2020.05.001.

716 24. Gazdar, A.F., Bunn, P.A., and Minna, J.D. (2017). Small-cell lung cancer: what we
717 know, what we need to know and the path forward. Nat Rev Cancer *17*, 725-737.
718 10.1038/nrc.2017.87.
719 25. Gazdar, A.F., Carney, D.N., Nau, M.M., and Minna, J.D. (1985). Characterization of
720 variant subclasses of cell lines derived from small cell lung cancer having distinctive
721 biochemical, morphological, and growth properties. Cancer Res *45*, 2924-2930.
722 26. Jiang, L., Huang, J., Higgs, B.W., Hu, Z., Xiao, Z., Yao, X., Conley, S., Zhong, H., Liu,
723 Z., Brohawn, P., et al. (2016). Genomic Landscape Survey Identifies SRSF1 as a Key
724 Oncodriver in Small Cell Lung Cancer. PLoS Genet *12*, e1005895.
725 10.1371/journal.pgen.1005895.
726 27. Wagner, A.H., Devarakonda, S., Skidmore, Z.L., Krysiak, K., Ramu, A., Trani, L.,
727 Kunisaki, J., Masood, A., Waqar, S.N., Spies, N.C., et al. (2018). Recurrent WNT
728 pathway alterations are frequent in relapsed small cell lung cancer. Nat Commun *9*, 3787.
729 10.1038/s41467-018-06162-9.
730 28. Jo, U., and Pommier, Y. (2022). Structural, molecular, and functional insights into
731 Schlafen proteins. Experimental & Molecular Medicine. 10.1038/s12276-022-00794-0.
732 29. Murai, J., Thomas, A., Miettinen, M., and Pommier, Y. (2019). Schlafen 11 (SLFN11), a
733 restriction factor for replicative stress induced by DNA-targeting anti-cancer therapies.
734 Pharmacol Ther *201*, 94-102. 10.1016/j.pharmthera.2019.05.009.
735 30. Masuda, K., Yoshida, T., Motoi, N., Shinno, Y., Matsumoto, Y., Okuma, Y., Goto, Y.,
736 Horinouchi, H., Yamamoto, N., Watanabe, S.-i., et al. (2025). Schlafen 11 Expression in
737 Patients With Small Cell Lung Cancer and Its Association With Clinical Outcomes.
738 Thoracic Cancer *16*, e15529. https://doi.org/10.1111/1759-7714.15529.
739 31. Dowlati, A., Chiang, A.C., Cervantes, A., Babu, S., Hamilton, E., Wong, S.F.,
740 Tazbirkova, A., Sullivan, I.G., van Marcke, C., Italiano, A., et al. (2025). Phase 2 Open-
741 Label Study of Sacituzumab Govitecan as Second-Line Therapy in Patients With
742 Extensive-Stage SCLC: Results From TROPiCS-03. J Thorac Oncol.
743 10.1016/j.jtho.2024.12.028.
744 32. Ahn, M.-J., Cho, B.C., Felip, E., Korantzis, I., Ohashi, K., Majem, M., Juan-Vidal, O.,
745 Handzhiev, S., Izumi, H., Lee, J.-S., et al. (2023). Tarlatamab for Patients with
746 Previously Treated Small-Cell Lung Cancer. New England Journal of Medicine *389*,
747 2063-2075. 10.1056/NEJMoa2307980.
748 33. Sun, N.Y., Kumar, S., Kim, Y.S., Varghese, D., Mendoza, A., Nguyen, R., Okada, R.,
749 Reilly, K., Widemann, B., Pommier, Y., et al. (2025). Identification of DLK1, a Notch
750 ligand, as an immunotherapeutic target and regulator of tumor cell plasticity and
751 chemoresistance in adrenocortical carcinoma. Nat Commun *16*, 5511.
752 10.1101/2024.10.09.617077.
753 34. Han, K., Chen, Y., Sun, X., Wen, L., Wu, Y., Chen, S., Wei, L., Yu, J., Zeng, T., Jiang,
754 L., and Tan, L. (2025). Combining serum CDK1 with tumor markers for the diagnosis of
755 small cell lung cancer. Clin Transl Oncol *27*, 2005-2013. 10.1007/s12094-024-03722-y.
756 35. Muley, T., Herth, F.J., Heussel, C.P., Kriegsmann, M., Thomas, M., Meister, M.,
757 Schneider, M.A., Wehnl, B., Mang, A., and Holdenrieder, S. (2024). Prognostic value of
758 tumor markers ProGRP, NSE and CYFRA 21-1 in patients with small cell lung cancer
759 and chemotherapy-induced remission. Tumour Biol *46*, S219-S232. 10.3233/TUB-
760 230016.

761 36. Kudoh, S., Tenjin, Y., Kameyama, H., Ichimura, T., Yamada, T., Matsuo, A., Kudo, N.,
762 Sato, Y., and Ito, T. (2020). Significance of achaete-scute complex homologue 1
763 (ASCL1) in pulmonary neuroendocrine carcinomas; RNA sequence analyses using small
764 cell lung cancer cells and Ascl1-induced pulmonary neuroendocrine carcinoma cells.
765 Histochem Cell Biol *153*, 443-456. 10.1007/s00418-020-01863-z.
766 37. Ajay, A., Wang, H., Rezvani, A., Savari, O., Grubb, B.J., McColl, K.S., Yoon, S., Joseph,
767 P.L., Kopp, S.R., Kresak, A.M., et al. (2025). Assessment of targets of antibody drug
768 conjugates in SCLC. NPJ Precis Oncol *9*, 1. 10.1038/s41698-024-00784-7.
769 38. Qu, S., Fetsch, P., Thomas, A., Pommier, Y., Schrump, D.S., Miettinen, M.M., and Chen,
770 H. (2022). Molecular Subtypes of Primary SCLC Tumors and Their Associations With
771 Neuroendocrine and Therapeutic Markers. J Thorac Oncol *17*, 141-153.
772 10.1016/j.jtho.2021.08.763.
773 39. Sun, F.D., and Das, M.S. (2024). Targeting the EZH2-SLFN11 pathway-a lesson in
774 developing molecularly-informed treatments for recurrent small cell lung cancer.
775 Translational Cancer Research *13*, 6608-6612. 10.21037/tcr-24-1755.
776 40. Zhang, B., Stewart, C.A., Wang, Q., Cardnell, R.J., Rocha, P., Fujimoto, J., Solis Soto,
777 L.M., Wang, R., Novegil, V., Ansell, P., et al. (2022). Dynamic expression of Schlafen
778 11 (SLFN11) in circulating tumour cells as a liquid biomarker in small cell lung cancer.
779 Br J Cancer. 10.1038/s41416-022-01811-9.
780 41. Kundu, K., Cardnell, R.J., Zhang, B., Shen, L., Stewart, C.A., Ramkumar, K., Cargill,
781 K.R., Wang, J., Gay, C.M., and Byers, L.A. (2021). SLFN11 biomarker status predicts
782 response to lurbinectedin as a single agent and in combination with ATR inhibition in
783 small cell lung cancer. Transl Lung Cancer Res *10*, 4095-4105. 10.21037/tlcr-21-437.
784 42. Laroche-Clary, A., Chaire, V., Valverde, V., Derieppe, M.A., and Italiano, A. (2025).
785 Synergistic Effects of ATR Inhibition and Lurbinectedin in Soft-Tissue Sarcomas: The
786 Predictive Role of SLFN11 Expression. Clin Cancer Res. 10.1158/1078-0432.CCR-24-
787 2556.
788 43. Thomas, A., Tanaka, M., Trepel, J., Reinhold, W.C., Rajapakse, V.N., and Pommier, Y.
789 (2017). Temozolomide in the Era of Precision Medicine. Cancer Res *77*, 823-826.
790 10.1158/0008-5472.CAN-16-2983.
791 44. Schultz, C.W., Zhang, Y., Elmeskini, R., Zimmermann, A., Fu, H., Murai, Y., Wangsa,
792 D., Kumar, S., Takahashi, N., Atkinson, D., et al. (2023). ATR inhibition augments the
793 efficacy of lurbinectedin in small-cell lung cancer. EMBO Molecular Medicine *15*,
794 e17313. https://doi.org/10.15252/emmm.202217313.
795 45. Gao, J., Aksoy, B.A., Dogrusoz, U., Dresdner, G., Gross, B., Sumer, S.O., Sun, Y.,
796 Jacobsen, A., Sinha, R., Larsson, E., et al. (2013). Integrative analysis of complex cancer
797 genomics and clinical profiles using the cBioPortal. Sci Signal *6*, pl1.
798 10.1126/scisignal.2004088.
799 46. Goldman, M.J., Craft, B., Hastie, M., Repečka, K., McDade, F., Kamath, A., Banerjee,
800 A., Luo, Y., Rogers, D., Brooks, A.N., et al. (2020). Visualizing and interpreting cancer
801 genomics data via the Xena platform. Nat Biotechnol *38*, 675-678. 10.1038/s41587-020-
802 0546-8.
803 47. Tang, Z., Kang, B., Li, C., Chen, T., and Zhang, Z. (2019). GEPIA2: an enhanced web
804 server for large-scale expression profiling and interactive analysis. Nucleic Acids Res *47*,
805 W556-W560. 10.1093/nar/gkz430.

806 48. Chandrashekar, D.S., Karthikeyan, S.K., Korla, P.K., Patel, H., Shovon, A.R., Athar, M.,
807 Netto, G.J., Qin, Z.S., Kumar, S., Manne, U., et al. (2022). UALCAN: An update to the
808 integrated cancer data analysis platform. Neoplasia *25*, 18-27.
809 10.1016/j.neo.2022.01.001.
810 49. Polley, E., Kunkel, M., Evans, D., Silvers, T., Delosh, R., Laudeman, J., Ogle, C.,
811 Reinhart, R., Selby, M., Connelly, J., et al. (2016). Small Cell Lung Cancer Screen of
812 Oncology Drugs, Investigational Agents, and Gene and microRNA Expression. J Natl
813 Cancer Inst *108*. 10.1093/jnci/djw122.
814 50. Simpson, K.L., Rothwell, D.G., Blackhall, F., and Dive, C. (2025). Challenges of small
815 cell lung cancer heterogeneity and phenotypic plasticity. Nat Rev Cancer *25*, 447-462.
816 10.1038/s41568-025-00803-0.
817 51. Chan, J.M., Quintanal-Villalonga, Á., Gao, V.R., Xie, Y., Allaj, V., Chaudhary, O.,
818 Masilionis, I., Egger, J., Chow, A., Walle, T., et al. (2021). Signatures of plasticity,
819 metastasis, and immunosuppression in an atlas of human small cell lung cancer. Cancer
820 Cell *39*, 1479-1496.e1418. https://doi.org/10.1016/j.ccell.2021.09.008.
821 52. Lissa, D., Takahashi, N., Desai, P., Manukyan, I., Schultz, C.W., Rajapakse, V., Velez,
822 M.J., Mulford, D., Roper, N., Nichols, S., et al. (2022). Heterogeneity of neuroendocrine
823 transcriptional states in metastatic small cell lung cancers and patient-derived models.
824 Nat Commun *13*, 2023. 10.1038/s41467-022-29517-9.
825 53. Stewart, C.A., Gay, C.M., Xi, Y., Sivajothi, S., Sivakamasundari, V., Fujimoto, J.,
826 Bolisetty, M., Hartsfield, P.M., Balasubramaniyan, V., Chalishazar, M.D., et al. (2020).
827 Single-cell analyses reveal increased intratumoral heterogeneity after the onset of therapy
828 resistance in small-cell lung cancer. Nature Cancer. 10.1038/s43018-019-0020-z.
829 54. Zhang, W., Girard, L., Zhang, Y.A., Haruki, T., Papari-Zareei, M., Stastny, V., Ghayee,
830 H.K., Pacak, K., Oliver, T.G., Minna, J.D., and Gazdar, A.F. (2018). Small cell lung
831 cancer tumors and preclinical models display heterogeneity of neuroendocrine
832 phenotypes. Transl Lung Cancer Res *7*, 32-49. 10.21037/tlcr.2018.02.02.
833 55. Ireland, A.S., Hawgood, S.B., Xie, D.A., Barbier, M.W., Lucas-Randolph, S., Tyson,
834 D.R., Zuo, L.Y., Witt, B.L., Govindan, R., Dowlati, A., et al. (2024). Basal cell of origin
835 resolves neuroendocrine–tuft lineage plasticity in cancer. bioRxiv,
836 2024.2011.2013.623500. 10.1101/2024.11.13.623500.
837 56. Qi, J., Zhang, J., Liu, N., Zhao, L., and Xu, B. (2022). Prognostic Implications of
838 Molecular Subtypes in Primary Small Cell Lung Cancer and Their Correlation With
839 Cancer Immunity. Front Oncol *12*, 779276. 10.3389/fonc.2022.779276.
840 57. Borromeo, M.D., Savage, T.K., Kollipara, R.K., He, M., Augustyn, A., Osborne, J.K.,
841 Girard, L., Minna, J.D., Gazdar, A.F., Cobb, M.H., and Johnson, J.E. (2016). ASCL1 and
842 NEUROD1 Reveal Heterogeneity in Pulmonary Neuroendocrine Tumors and Regulate
843 Distinct Genetic Programs. Cell Rep *16*, 1259-1272. 10.1016/j.celrep.2016.06.081.
844 58. Choudhury, N.J., Lai, W.V., Makhnin, A., Heller, G., Eng, J., Li, B., Preeshagul, I.,
845 Santini, F.C., Offin, M., Ng, K., et al. (2024). A Phase I/II Study of Valemetostat (DS-
846 3201b), an EZH1/2 Inhibitor, in Combination with Irinotecan in Patients with Recurrent
847 Small-Cell Lung Cancer. Clin Cancer Res *30*, 3697-3703. 10.1158/1078-0432.CCR-23-
848 3383.
849 59. Rudin, C.M., Reck, M., Johnson, M.L., Blackhall, F., Hann, C.L., Yang, J.C., Bailis,
850 J.M., Bebb, G., Goldrick, A., Umejiego, J., and Paz-Ares, L. (2023). Emerging therapies

851 targeting the delta-like ligand 3 (DLL3) in small cell lung cancer. J Hematol Oncol *16*,
852 66. 10.1186/s13045-023-01464-y.
853 60. Paul, S., Konig, M.F., Pardoll, D.M., Bettegowda, C., Papadopoulos, N., Wright, K.M.,
854 Gabelli, S.B., Ho, M., van Elsas, A., and Zhou, S. (2024). Cancer therapy with
855 antibodies. Nat Rev Cancer *24*, 399-426. 10.1038/s41568-024-00690-x.
856 61. Shen, L., Sun, X., Chen, Z., Guo, Y., Shen, Z., Song, Y., Xin, W., Ding, H., Ma, X., Xu,
857 W., et al. (2024). ADCdb: the database of antibody-drug conjugates. Nucleic Acids Res
858 *52*, D1097-D1109. 10.1093/nar/gkad831.
859 62. DeLucia, D.C., Cardillo, T.M., Ang, L., Labrecque, M.P., Zhang, A., Hopkins, J.E., De
860 Sarkar, N., Coleman, I., da Costa, R.M.G., Corey, E., et al. (2021). Regulation of
861 CEACAM5 and Therapeutic Efficacy of an Anti-CEACAM5-SN38 Antibody-drug
862 Conjugate in Neuroendocrine Prostate Cancer. Clin Cancer Res *27*, 759-774.
863 10.1158/1078-0432.CCR-20-3396.
864 63. Du, Y., Wen, Y., and Huang, J. (2024). Analysis of variation of serum CEA, SCC,
865 CYFRA21-1 in patients with lung cancer and their diagnostic value with EBUS-TBNA. J
866 Med Biochem *43*, 363-371. 10.5937/jomb0-37083.
867 64. Yu, M., and Wang, P. (2024). A comparative study of ProGRP and CEA as serological
868 markers in small cell lung cancer treatment. Discov Oncol *15*, 485. 10.1007/s12672-024-
869 01323-3.
870 65. Kim, Y.S., Nabet, B.Y., Cortez, B.N., Sun, N.Y., Sebastian, R., Redon, C.E., Ray, A.,
871 Liu, L., Ishola, A.A., Loew, S., et al. (2025). NOTCH1 reverses immune suppression in
872 small cell lung cancer through reactivation of STING. J Clin Invest *135*.
873 10.1172/JCI185423.
874 66. Roper, N., Velez, M.J., Chiappori, A., Kim, Y.S., Wei, J.S., Sindiri, S., Takahashi, N.,
875 Mulford, D., Kumar, S., Ylaya, K., et al. (2021). Notch signaling and efficacy of PD-
876 1/PD-L1 blockade in relapsed small cell lung cancer. Nat Commun *12*, 3880.
877 10.1038/s41467-021-24164-y.
878 67. Mayakonda, A., Lin, D.C., Assenov, Y., Plass, C., and Koeffler, H.P. (2018). Maftools:
879 efficient and comprehensive analysis of somatic variants in cancer. Genome Res *28*,
880 1747-1756. 10.1101/gr.239244.118.
881
882
883
884 **BioRxiv link: doi:** https://doi.org/10.1101/2025.07.07.663501
885
886 **Author Contributions:** Y.P. supervised the study. Y.P., F.E., Y.A., devised the concept. Y.A.,
887 D.T., A.T., A.L., J.D.R, F.A., K.A. and M.R. data collection and clinical annotations. Y.P., F.E.,
888 A.D., S.V., D.T., Y.A., A.L., R.S., N.R., A.T., C.R., A.T. and W.R performed data analysis. F.E.,
889 J.W. and A.Te. built the website. Y.P., F.E., A.D., A.L., A.T., M.A., N.R., C.R., W.R wrote and
890 critically reviewed the manuscript. All authors reviewed the results and approved the final version
891 of the manuscript.
892
893 **Funding:** Our work is funded by Center for Cancer Research, the Intramural Program of the
894 National Cancer Institute, NIH (Z01-BC 006150). In addition, this work is supported by the
895 Division of Intramural Research (DIR) of the National Library of Medicine (NLM)
896 (ZIALM240126).
897

898 **Data Availability Statement:** The clinical information for all four datasets provided in
899 Supplementary Data and normalized FPKM expression data is available at
900 https://discover.nci.nih.gov/SclcTumorMinerCDB/.
901
902 **Acknowledgments:** Our work is supported by Center for Cancer Research, National Library of
903 Medicine and Developmental Therapeutics Branch, National Cancer Institute. We thank the NCI
904 CCR Collaborative Bioinformatics resource (CCBR) team for their help in running the RNA-seq
905 and Exome-seq pipelines.
906
907 **Declaration of Interest:** The authors declare no competing interests.
908

909 **Table 1.** SCLC samples and Datasets
910
911

		Untreated		Relapse	
		UoC	**TU**	**NCI**	**Total**
Number of Samples		56	98	50	204
Genomics	RNA Seq	56	98	50	204
	WES	0	98	16	114
Prior Treatment	Yes	0	0	50	50
	No	52	98	0	150
	Unknown	4	0	0	4
Biopsy Site	Lung	55	98	7	160
	Liver	0	0	21	21
	Lymph Node	0	0	10	10
	Pleura	1	0	1	2
	Adrenal Gland	0	0	4	4
	Mediastinal mass	0	0	3	3
	Others	0	0	4	4
Tumor Stage	Stage 1	25	30	0	55
	Stage 2	7	26	0	33
	Stage 3	17	41	2	60
	Stage 4	7	1	48	56

912
913

Figures with legends

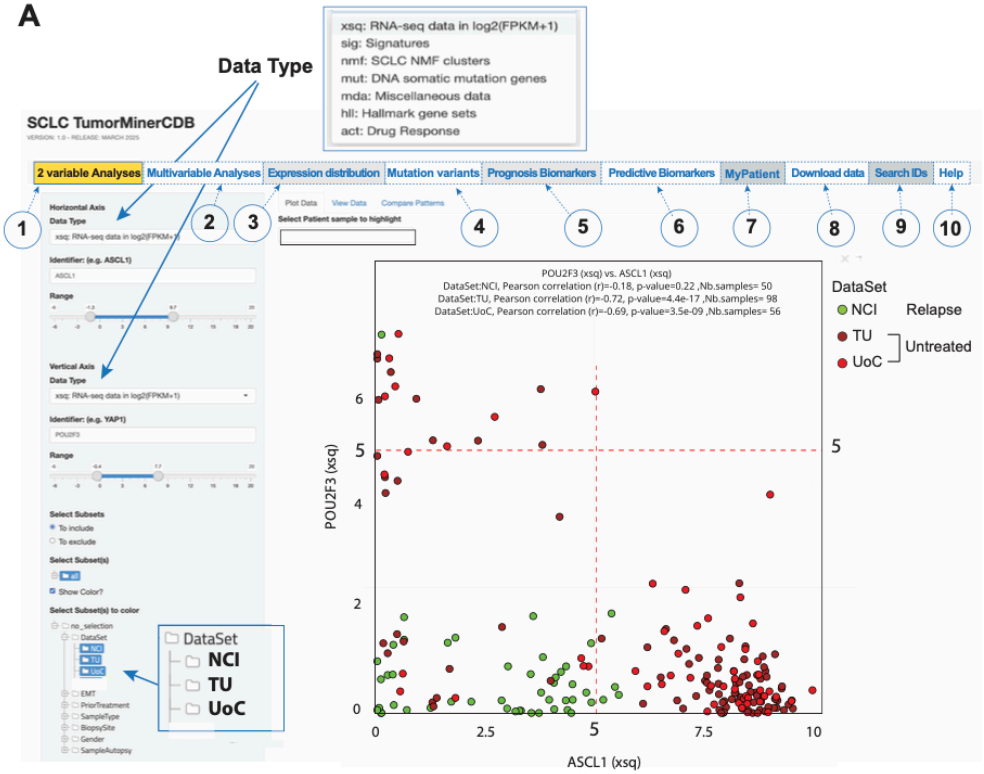

B

	NEUROD1	ASCL1	POU2F3	YAP1	ASCL1 +NEUROD1
Untreated [1]	24% (37)*	**75% (115)***	10% (16)*	2% (3)*	5% (29)*
Relapse [2]	12% (6)*	8% (4)*	2% (1)*	**22% (11)***	0
Cell lines [3]	20% (10)*	**56% (28)***	8% (4)*	8% (4)*	4% (2)*

* Number of samples are in parenthesis
[1] All untreated samples can be assigned to a NAPY group
[2] Only 44% of relapse samples can be assigned to a NAPY group
[3] 92% of the SCLC cell lines from CCLE can be assigned to a NAPY group

Figure 1. Introduction to SCLC TumorMiner (https://discover.nci.nih.gov/SclcTumorMinerCDB/). **A**. Snapshot of the introductory "2 variable Analyses" display (1). Both the horizontal and vertical axes offer a choice of "Data Type" shown in the upper inset. Users must type their choice in the "Identifier" box (here ASCL1 for the horizontal axis and POU2F3 for the vertical axis). Other options include choosing the "Range" for the axes and the "Select Subsets" to "include" or "exclude". The + sign and folder indicate that further selections can be made such as choosing the "Dataset" to display. To display more than one dataset, users need to press the Command key while clicking the individual datasets (lower inset). Other features of SCLC TumorMiner include: (2) "Multivariable Analyses" with examples shown in Figure 2; (3) "Expression Distribution" across the 4 Datasets with example shown in Figure S1; (4) "Mutation variants"; (5) "Prognosis Biomarkers" with example shown in Figures 5 and S4; (6) "Predictive Biomarkers" with example shown in Figure 6; (7) "My Patient" to display the genomic characteristics of a selected patient with example shown in Figures 7 and S6. Additional features include the ability to "Download Data" for further analyses (8) as shown in Figures 7, S1, S4 and S5, "Search IDs" (9), as well as a detailed "Help" section (10). **B**. NAPY distribution of samples from untreated and relapse patients and from the SCLC cell lines (https://discover.nci.nih.gov/SclcCellMinerCDB) [4]. Samples were assigned to each NAPY group based on gene expression log2(FPKM+1) > 5.0 (see horizontal and vertical dotted lines in panel A and justification for the > 5.0 threshold in Figure S1).

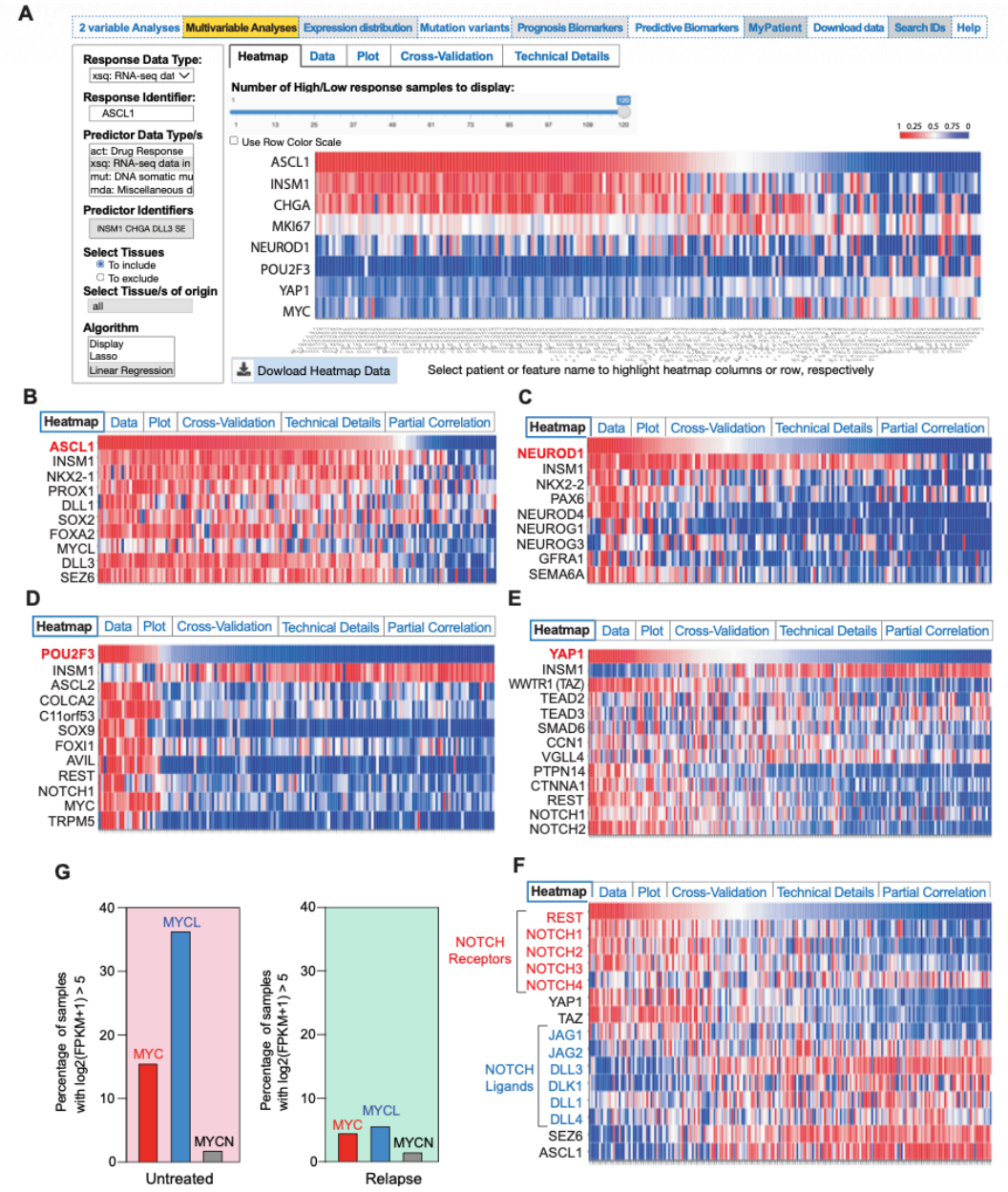

Figure 2. Multivariable Analyses showing co-regulation of the neuroendocrine (INSM1, CHGA), NAPY (NEUROD1, ASCL1, POU2F3 and YAP1), NOTCH (NOTCH1, NOTCH2, REST) and MYC (MYC, MYCL and MYCN) pathways. **A**. Default display for the "Multivariable Analyses" tab. Color scale goes from red to blue to reflect expression levels for each gene (rows) and patients (columns). Users can choose different data types (upper inset of panel A) and then type the "Response Identifier" to display as the first row on the heatmap. "Predictor Identifier (s)" need to be typed with a space between each. "Tissues of origin" can be selected. The default algorithm (bottom left) is "Display". Users can also perform Linear and Lasso analyses like in CellMinerCDB (https://discover.nci.nih.gov/cellminercdb/). **B-E**. Multivariable analyses for the NAPY genes used as "Response Identifiers". I*NSM1* is included in each analysis as a NE biomarker. Panels B-D only include the samples from the databases of untreated patients. **F**. Multivariable analysis for the Notch pathway. **G**. Differential expression of the 3 MYC genes in samples from untreated and relapse patients. Linear regression analyses for each of "Response Identifiers" (in red, 1st rows in panels B-F) show that the "Predictor Identifiers" are highly significant (see Figure S2C).

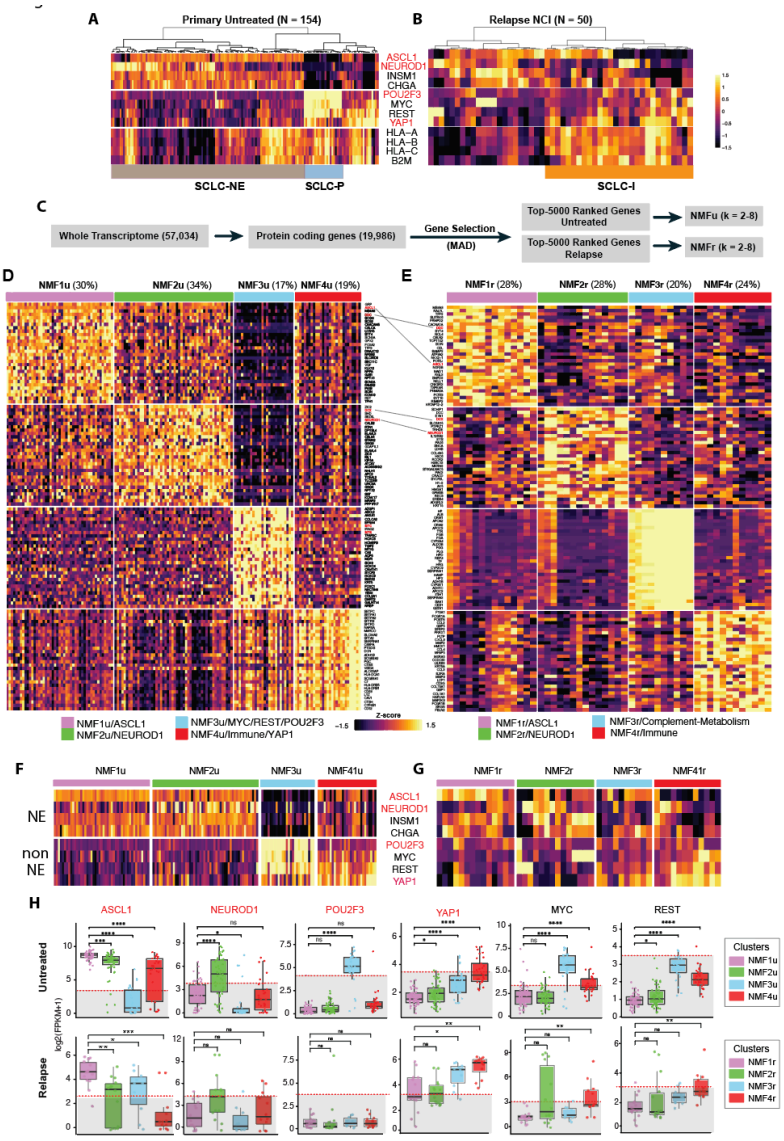

Figure 3. Classification of the untreated (primary) and relapse 204 SCLC samples comparing untreated (UoC and TU datasets) and relapse samples (NCI). **A-B**. Hierarchical clustering of the untreated and relapse samples based on the expression of the four genes of the NAPY classification (*NEUROD1*, *ASCL1*, *POU2F3* and *YAP1* in red) and of genes reflecting commonly used biomarkers for clinical neuroendocrine (NE) classification (*INSM1* and *CHGA*) as well as *MYC*, *REST* and 4 exemplary innate immune genes (*HLA-A*, *HLA-B*, *HLA-C* and *B2M)*. **C**. Flow chart summarizing the NMF approach for selecting 5,000 protein-coding transcripts based on MAD (Median Absolute Deviation) for the untreated and relapse samples. **D-E**. Display of the NMF clusters for the untreated and relapse samples (D and E, respectively). The percentages of samples within each NMF are indicated in parenthesis. NMFs for untreated and relapse are abbreviated NMFu and NMFr, respectively. The rows show the top 30 genes for each NMF with log fold-change > 1 and p-value < 0.05. Genes that are common across untreated and relapse samples for the NMF clusters are indicated by the oblique lines. **F-G**. NMF distribution of the canonical NAPY genes (red) and reference NE genes as well as *MYC* and *REST*. **H**. Box plots comparing the differential expression of the NAPY genes, *MYC* and *REST* across the 4 untreated (top) and relapse NMFs (bottom). Statistical comparisons were performed by Student t-test. **** indicates $p < 0.001$; ** $p < 0.01$; * $p < 0.05$. Shaded areas represent low expression (log2(FPKM+1) <3).

C

Signature_mean	NMF1u	NMF2u	NMF3u	NMF4u	NMF1r	NMF2r	NMF3r	NMF4r
NE	0.53	0.63	-0.41	-0.38	0.66	0.31	-0.31	-0.24
RepStress	0.03	0.49	-0.01	-0.53	0.36	0.62	-0.58	-0.28
CES	0.01	0.70	-0.03	-0.53	0.32	0.53	-0.45	-0.33
Epithelial	0.62	-0.22	0.43	0.11	0.42	-0.41	0.19	0.05
Stroma	-0.20	-0.19	0.27	0.93	-0.20	-0.31	0.25	0.93
Immune	-0.11	-0.34	0.28	0.92	-0.23	-0.53	0.24	0.90
APM	0.07	-0.43	0.31	0.70	-0.17	-0.41	0.24	0.66
Ychrom	-0.13	-0.01	-0.18	0.32	-0.16	0.14	0.19	0.18

Figure 4. Genomic signatures associated with each NMF from the untreated and relapse patient biopsy samples. **A-B**. Reactome pathway analyses for untreated and relapse samples. **B**. Correlation between each of the NMF's and the eight genomic signatures of SCLC TumorMiner for the samples from untreated (left) and relapse (right) patients. Correlations were obtained using the "2 variable Analyses" of the SCLC TumorMiner website ("Plot Data" or "View Data" tabs for each of the NMF on the horizontal axis). For the untreated samples the corresponding NMF's were computed after limiting the analysis using "Select Subsets" for the untreated Datasets: TU + UoC. Conversely for the relapse samples, analyses were done using the NCI samples:

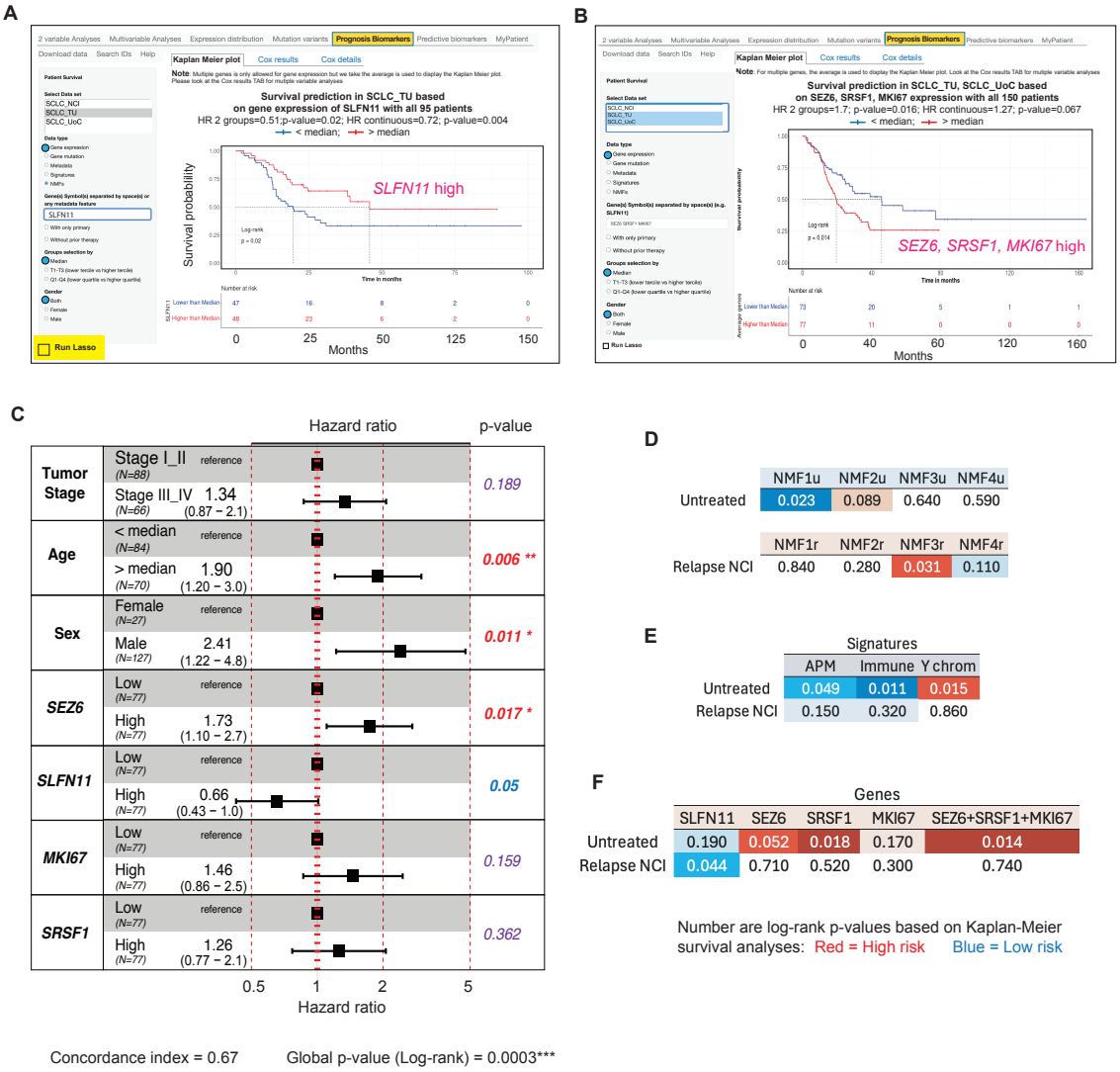

Figure 5. Exploration of prognosis biomarkers. Panels A and F are screen snapshot of the SCLC TumorMiner website. **A**. High *SLFN11* expression is a good prognosis biomarker for the untreated TU Dataset. **B**. Combined expression of *SEZ6*, *SRSF1* and *MKI67* are significant risk factors for the combined untreated datasets (TU & UoC). **C**. Multivariate survival analysis including *SEZ6, SLFN11*, *SRSF1*, *MKI67* expression, age, tumor stage and sex for the untreated patients (TU and UoC datasets). **D**. Tabulated results for the prognosis value of each NMF cluster. **E**. Prognostic value of 3 of the 8 signatures of SCLC TumorMiner. **F**. Prognostic value of *SLFN11*, *SEZ6, MKI67* and combined expression of *SEZ6*, *SRSF1* and *MKI67* as prognosis biomarkers for the untreated and relapse datasets. Numbers (panels D-F) are log-rank p-values based on Kaplan-Meier survival analysis and colors highlight significant value ($p < 0.05$) with low-risk parameter in blue and high-risk in red.

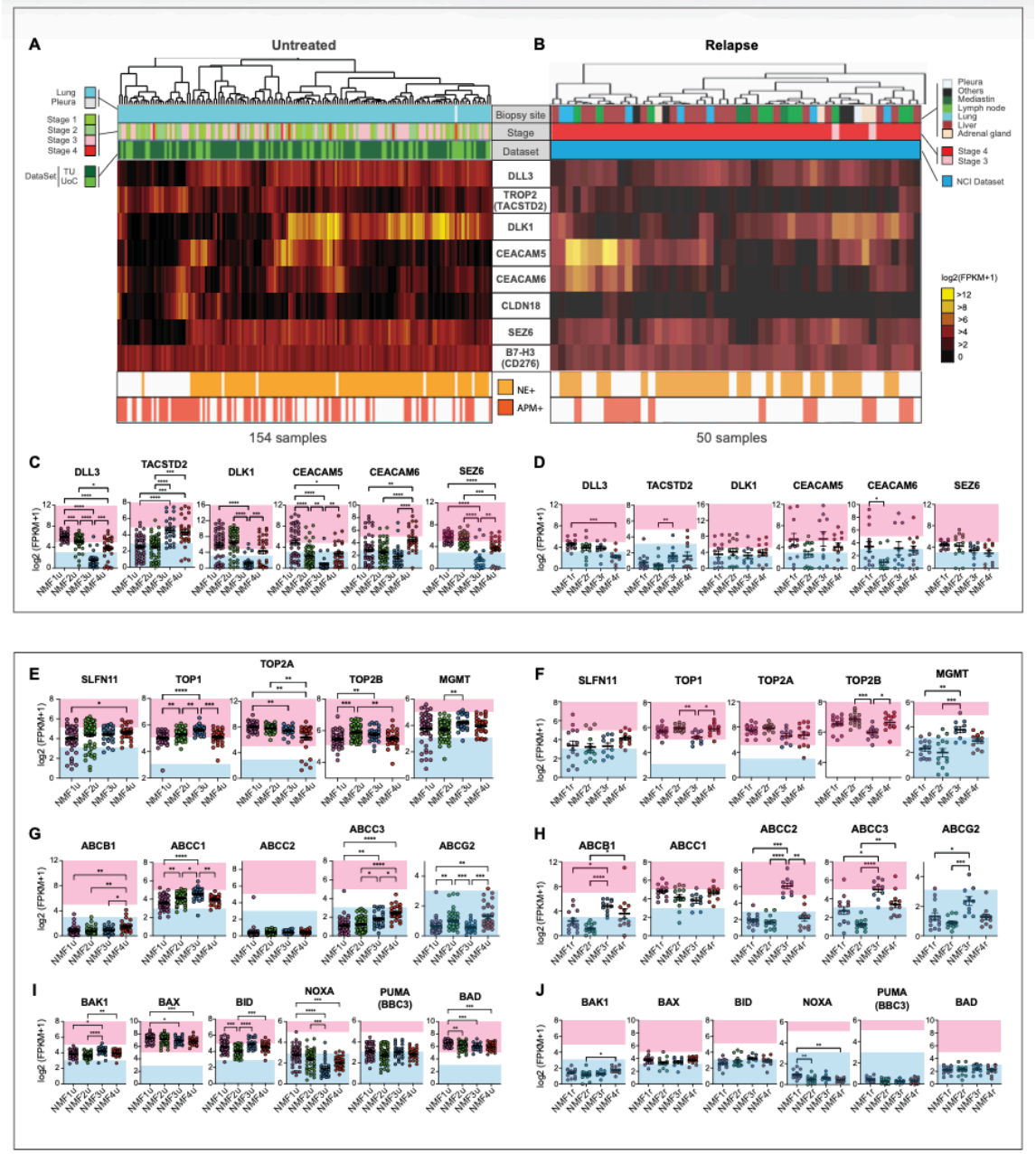

Figure 6. Predictive biomarkers with focus on ADCs for untreated patients (left panels A, C, E, G & I) versus patients after relapse (right panels B, D, F, H & J). **A-B**. Heatmaps showing the differential expression of 8 selected ADC targets. Samples were clustered based on the ADC target surface receptor genes listed between panels A and B. DLL3 and TROP2 (TACSTD2) are both FDA-approved targets. Expression of *DLK1*, *CEACAM5*, *CEACAM6*, *CLN18*, *SEZ6* and *B7H3* are displayed because of their selective expression in subsets of patients. The top parts of the figure show for each patient the biopsy site, clinical stage, sample type and dataset. The bottom part shows for each patient whether the sample is enriched for the neuroendocrine (NE) and antigen-presenting-machinery (APM) signatures. **C-D**. Relationship between the listed ADC antibody targets and the NMF subgroups (NMFu and NMFr stand for the NMFs of samples from untreated and relapse patients, respectively. The blue-shaded areas include samples with low gene expression (log2(FPKM+1) <3) and the pink-shaded areas samples with high expression (log2(FPKM+1) >5). **E-F**. Expression of drug targets/biomarkers in the different NMF subgroups. **G-H**. Expression of drug efflux transporters. **I-J**. Expression of major pro-apoptotic genes in the different NMF subgroups. Statistical comparisons were performed by Student t-test. **** indicates $p < 0.001$; ** $p < 0.01$; * $p < 0.05$.

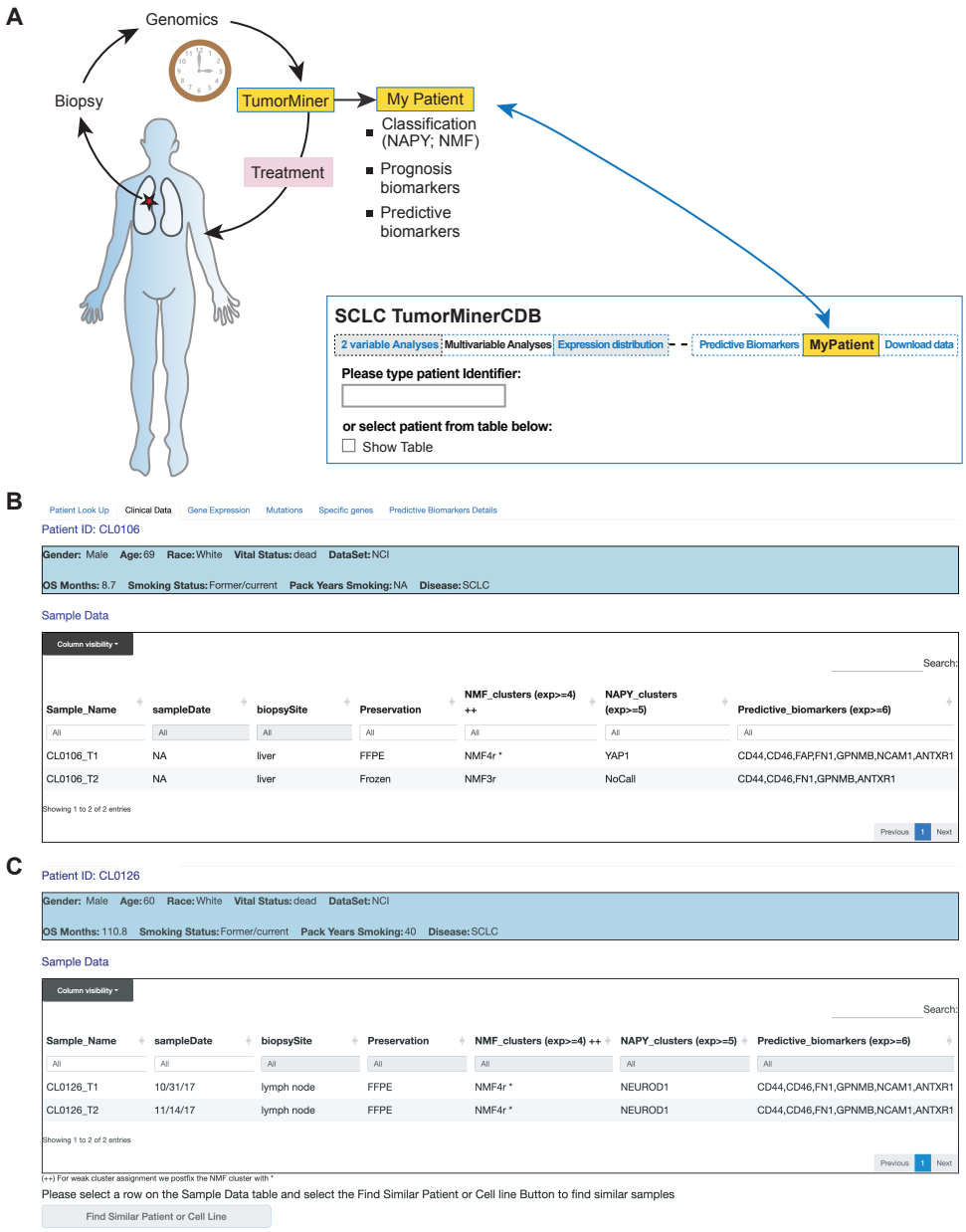

Figure 7. MyPatient module of SCLC TumorMiner. **A**. Proposed use of the "MyPatient" module. Genomic analyses are performed immediately after biopsy and uploaded into Tumor_Miner to provide results guiding the patient treatment as genomic classification, prognostic and predictive biomarkers are automatically displayed using "MyPatient" tab. **B**. Snapshot of the "MyPatient" tab in SCLC TumorMiner. Users are prompted to enter a "patient identifier" or select a patient from the available table. Here the patient has two samples from liver biopsies: one frozen and the other from FFPE. **C**. Snapshot of the "MyPatient" tab for patient "CL0126" who has two lymph node biopsy samples taken at 2-week interval.

1011 **STAR METHODS**

1012

1013 **RESOURCE AVAILABILITY**

1014 **Lead Contact:** Further information and requests for reagents may be directed and will be fulfilled
1015 by Lead Contact Yves Pommier (yves.pommier@nih.gov)

1016 **Material Availability**: this study did not generate new unique reagents

1017 **Data and code Availability**

1018 - **Data:** the data used for the analysis can be downloaded from the website at
1019 https://discover.nci.nih.gov/SclcTumorMinerCDB/ or obtained from Zenodo at
1020 https://doi.org/10.5281/zenodo.18343141
1021 - **Code:** the website code is publicly available in GitHub at
1022 https://github.com/cbiit/SclcTumorMinerCDB
1023 - **Other:** Any additional information or script required to reanalyze the data reported in this
1024 paper is available from the lead contact upon request

1025

1026 **EXPERIMENTAL MODEL AND STUDY PARTICIPANT DETAILS**

1027 Patient clinical and genomics data were collected from our DTB clinic at the Center for Cancer
1028 Research, NCI-NIH, the University of Cologne (UoC) and Tongji university (TU). Our genomics
1029 patient data currently includes a total of 204 samples from 189 patients with RNA-seq and/or
1030 whole-exome sequencing (WES) samples. The NIH samples were obtained from patients enrolled
1031 in IRB-approved protocols and had consented to the analysis of their tumors. Clinical data from
1032 NIH and collaborators were gathered and manually curated by a team of DTB physicians. They
1033 integrate patient demographics, survival, treatment with response, and sample information,
1034 including sample type, biopsy site, tumor stage and pathology indicators (see Table S1). NCI
1035 patient samples were correlated with treatment response, and for each patient we selected the
1036 first drug(s) or treatment(s) post-sampling as well as its response class (CR: complete response,
1037 PR: partial response, PD: progressive disease or SD: stable disease). Due to the current limited
1038 number of treatments, we decided that the response will be of value 1 (good responder: PR, CR)
1039 or 0 (bad responder: SD, PD).
1040

1041 **METHOD DETAILS**

1042 **Genomic content and Infrastructure**
1043 All genomics patient data were processed with our on-site data-handling pipelines using the raw
1044 data. We generated 204 RNA-seq and 114 WES normalized data. Treatment responses were
1045 available for 14 patients. Table S11 shows details by disease, data sets and experiments.
1046 We also computed for each sample gene expression Hallmark enrichment and genomics signatures
1047 scores such as the NE, RepStress, EMT, APM, the level of stroma and immune infiltrate
1048 contamination or a new Y chromosome signature score. Table S12 presents the list of signatures
1049 as well as the phenotypic data queryable on SCLC TumorMiner.
1050 SCLC TumorMiner has similar design as the CellMinerCDB tool and websites
1051 (https://discover.nci.nih.gov/) dedicated to mining pharmaco-genomics data across broad ranges

of cancer cell line sets and databases. SCLC TumorMiner is implemented as a shiny application and hosted using Posit Connect on CBIIT servers at https://discover.nci.nih.gov/SclcTumorMinerCDB/.

RNA sequencing and batch assessment

The NIH/NCI (relapse) cohort was composed predominantly of FFPE specimens (n=42), with a limited number of frozen samples (n=8) using the Illumina access protocol, whereas the Universities of Cologne (UoC) and Tongji university (TU) were from Frozen using PolyA protocol. All the SCLC samples were processed by running the NCI CCBR RNAseq pipeline (https://github.com/skchronicles/RNA-seek.git). STAR (2.7.6a) was run to map reads to hg38 reference genome (release 36). Then RSEM was used to have gene expression values in log2(FPKM+1). For the NCI dataset, we checked whether the way the samples were preserved—Frozen or FFPE—affects gene expression, along with other factors like biopsy site, sex, and age. Analysis of the NCI samples including 8 frozen biopsy samples and 42 FFPE samples shows that preservation methods only explain 2.9% of the variance, which is quite low, especially compared to the biopsy site, which explains 10.8%. All untreated samples are frozen. Because the preservation method is confounded with sample type (relapse vs. untreated), its effect cannot be disentangled (See Figure S8). Thus, no batch effect was applied for all 3 datasets.

Mutations

Somatic mutations were based on paired tumor-normal samples and ran with the CCBR exome sequencing pipeline (https://github.com/mtandon09/CCBR_GATK4_Exome_Seq_Pipeline). Briefly, BWA MEM (version 0.7.17) was run to map reads to the hg38 reference genome. Then Mutect2 in GATK 4.2 was used to call the variants.

Across 98 Tongji University paired normal and tumor exomes, the median of the mean target depth was 161.57× (IQR 139.32–189.27×), and a median of 97.1% (IQR 96.2–97.7%) of target bases were covered at ≥30×. For NCI, across 16 paired normal and tumor exomes, the median of the mean target depth was 97.75× (IQR 62.9–143.5×), and a median of 90.9% (IQR 79.9–95.42%) of target bases were covered at ≥30×. Sample coverage details are provided in supplementary Tables S13 and S14.

Variants with 6 or more total filtered reads were selected for display. We used Annovar (hg38 version) to annotate the mutations, including their predicted effect on amino-acid sequence and whether they are predicted to be deleterious, as well as their prevalence in the ExAC normal population. A mutation was called deleterious if its predicted effect on the RNA sequence was frameshift, nonsense, splice-site, or a missense mutation with a SIFT score <0.05 or PolyPhen2 HDIV score>=0.85. We selected all deleterious variants for the mutation gene-level score.

The fraction of alternate alleles (the mutation ratio) was used as the probability that any cell has that mutation. Furthermore, we assumed that the probability that any mutation is present in a gene is independent of the probability of any other mutation on that gene. Given those assumptions, we calculate the overall mutation probability for that gene in any cell as:

$$1-(1-p1)*(1-p2)*...*(1-pn)$$

where p1, p2, ..., pn are the mutation ratios for each individual mutation on that gene. 1-pj is the probability that jth mutation is not present for a particular cell. Thus, the product is the probability that none of the mutations are present and 1 minus the product is the probability that at least one mutation is present. The expression gives a number that is between 0 and 1, which we multiply by 100 to get the mutation score for that gene.

1098
1099 **Tumor Mutation Burden (TMB)**
1100 The TMB was computed using the R package MAFtools [67] based on Mutect2 somatic variants that
1101 have variant allele frequency (VAF) >= 5%.
1102
1103 **Genomic data for survival**
1104 If a patient has multiple samples, we select the primary tumor sample (if available) for survival
1105 analysis or we choose one based on biopsy site. The list of selected samples is downloadable from
1106 the website.
1107
1108 **QUANTIFICATION AND STATISTICAL ANALYSIS**
1109 **Unsupervised Clustering Approach**
1110 We implemented unsupervised clustering based on Non-Negative Matrix Factorization (NMF)
1111 algorithm using log-transformed normalized RNA-seq data to classify SCLC patients into
1112 molecular subtypes. NMF uses dimensionality reduction approach in which it decomposes the
1113 gene expression matrix X (n × m), into the product of two lower-dimension non-negative matrices
1114 (See Equation below), where n represents number of patients and m is number of genes.
1115 $$X \approx WH$$
1116 with X = n × m matrix, W = n × k matrix, and H = m × k, where k is a latent factor; optimal number
1117 of factors (k) was determined based on matrix stability using cophenetic correlation coefficient.
1118 We selected only protein-coding genes for both untreated and relapse SCLC samples, then we
1119 selected the top 5000 highly variable genes for both datasets using a non-parametric approach,
1120 Median Absolute Deviation (MAD) using "mad" function in R (version 4.2.3). After which, we
1121 performed consensus NMF clustering evaluating values of k ranging from 2 to 8, based on
1122 cophenetic correlation coefficient. k = 4 provided most stable and robust clusters for both untreated
1123 and relapse SCLC datasets (See Figure S4). Clustering was performed using "NMF" library in R
1124 (version 4.2.3).
1125
1126 **Pairwise Differential Expression Analysis**
1127 After defining the NMF subgroups, differential gene analyses were performed using the "Limma"
1128 package in R (version 4.2.3). To determine the up or down-regulated genes across the NMF-
1129 subgroups, we performed pairwise comparisons for untreated and relapse SCLC separately. This
1130 included all possible combinations of comparisons: NMF1 vs NMF2, NMF1 vs NMF3, NMF3 vs
1131 NMF4, NMF2 vs NMF3, NMF2 vs NMF4, NMF3 vs NMF4. In addition, each subgroup was
1132 compared with the aggregated sum of other subgroups, for instance: NMF1 vs Others
1133 (NMF2+NMF3+NMF4), NMF2 vs Others (NMF1+NMF3+NMF4), NMF3 vs Others
1134 (NMF1+NMF2+NMF4) and NMF4 vs Others (NMF1+NMF2+NMF3).
1135 Subsequently, we utilized these pairwise comparisons to identify subgroup-specific genes
1136 for each NMF cluster for both untreated and relapse samples. Significantly upregulated genes in
1137 NMF1 in comparison to NMF2, NMF3 and NMF4 with $\log_2$FC >1 and p-value < 0.05 are listed
1138 as NMF1-specific genes. Similarly, this criterion was implemented for the selection of specific
1139 genes for the NMF2, NMF3 and NMF4 subgroups. The subgroup-specific genes identified using
1140 this approach were used to construct NMF-derived gene expression signatures.
1141
1142 **Gene Set Enrichment Analysis (GSEA)**

To investigate the functional relevance of genes we performed pre-ranked Gene Set Enrichment Analysis (GSEA). From previous analysis, we obtained pairwise comparisons for each NMF groups and used t-statistic parameter, which provided magnitude and direction of differential expression to rank the genes. Ranked genes were then analyzed using the fGSEA R package (version 4.2.3) with REACTOME gene sets [https://www.gsea-msigdb.org/gsea/msigdb/human/collections.jsp#C5]. fGSEA is a fast implementation of the GSEA algorithm providing normalized enrichment scores (NES) and adjusting for multiple testing using permutation-based p-values and false discovery rate (FDR).

Mypatient NMF cluster assignment

For each patient sample, we calculated the average expression of the four NMF signatures (see Figure S7). The assigned NMF cluster corresponds to the signature with the highest average expression, provided that this value is at least 4 (log2(FPKM+1)); otherwise, no cluster is assigned. If the highest average expression differs from the second highest by less than 1, the cluster assignment is considered weak and is labeled accordingly.

Statistical Methods

Correlations, scatter plots, heatmaps, survival analysis, regression model predictions, and pathway enrichment scores were generated using the R-Project for statistical computing based mostly on the R packages: ggplot2, plotly, heatmaply, survival, glmnet, ggforest, GSVA and GSEABase. These packages are downloadable from the comprehensive R archive network (CRAN) or Bioconductor websites.

1166 **KEY RESOURCES TABLE**

1167

REAGENT or	SOURCE	IDENTIFIER
Deposited data		
NIH NCI – Patient Data	Lissa et al, 2022 [52]	dbGAP: phs002541.v1.p1
SCLC tumor transcriptomic data	George et al, 2015 [2]	EGA:EGAS00001000925
Tongji SCLC data	Liu et al, 2024 [9]	https://ngdc.cncb.ac.cn/gsa-human/browse/HRA003419
Impower133 tumor transcriptomic data	Gay et al, 2021 [5]	EGA:EGAS00001004888
Wagner dataset	Wagner et al, 2018 [27]	dbGAP: phs001049.v1.p1
SCLC tumor transcriptomic data	Jiang et, 2016 [26]	GEO:GSE60052
Software and algorithms		
R version 4.5.1		www.r-project.org
Bioconductor		www.bioconductor.org
RNASeq pipeline	NCI CCBR	https://github.com/skchronicles/RNA-seek
Mutation pipeline	NCI CCBR	https://github.com/mtandon09/CCBR_GATK4_Exome_Seq_Pipeline
GSVA (version 2.4.4)		
fGSEA (version 4.2.3)		
NMF (version 0.28)		
Survival (version 3.8.3)		
GraphPad Prism	GraphPad	
Analysis scripts		
SCLC TumorMinerCDB	This paper	https://github.com/cbiit/SclcTumorMinerCDB

1168

Supplemental Figures

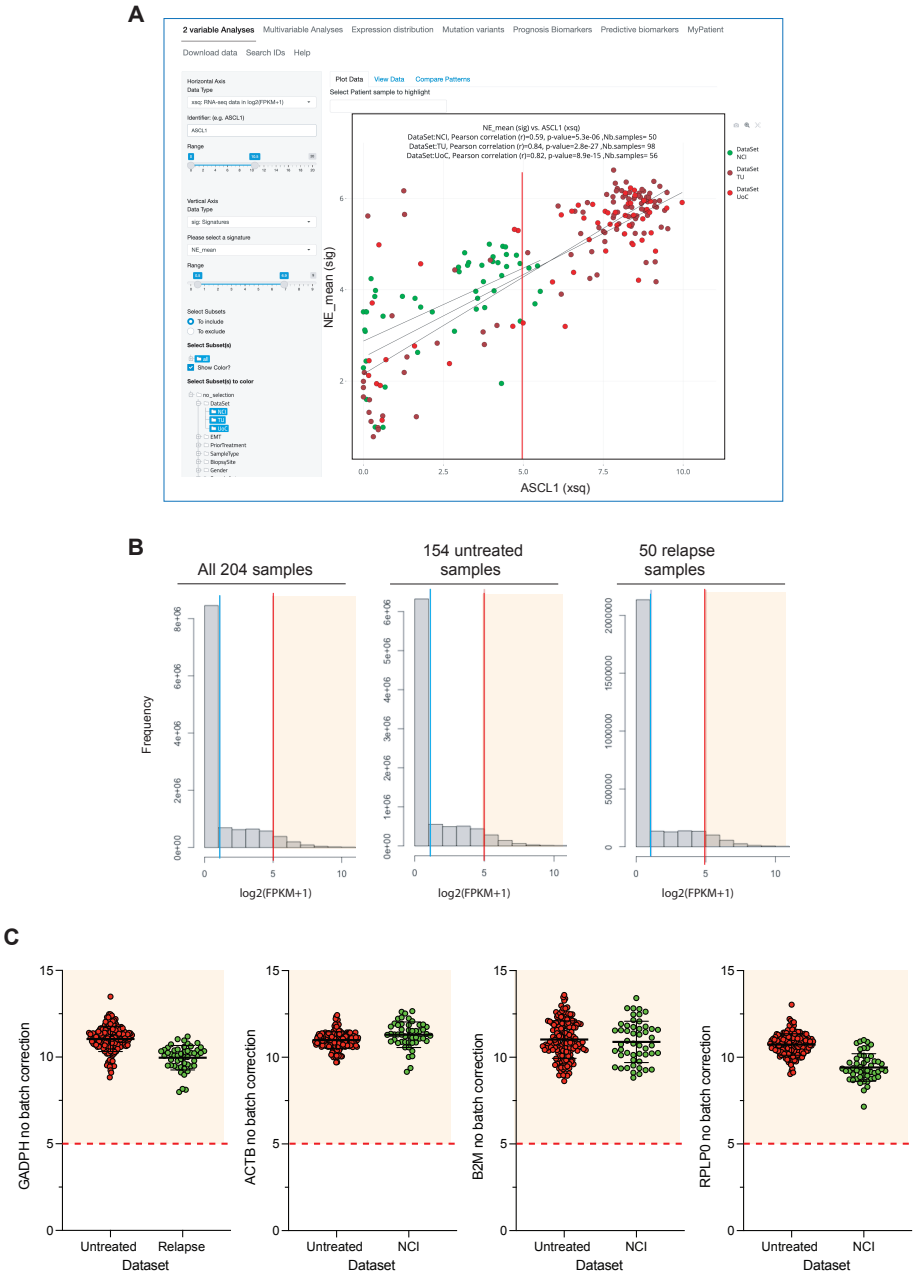

Figure S1 (related to Fig 1). **A**. Example of a "2 Variable Analysis" snapshot of the websites displaying the correlation between *ASCL1* expression and the NE signature. **B**. Frequency distribution of gene expression across the datasets. The red line indicates the >90% cutoff (log2(FPKM+1)>5) for high gene expression. **C**. Comparative expression of 4 canonical housekeeping genes in the untreated and relapse samples. Colored areas define samples with significant expression ((log2(FPKM+1) > 5.0 in pink). Data were downloaded from the SCLC TumorMiner website using the download tabs.

A

B

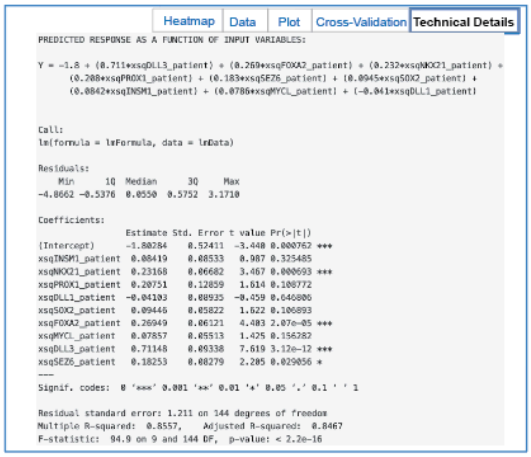

C

Predictive value for the listed Response Identifiers

Response identifier	**ASCL1** (panel A)	**ASCL1** (panel B)	**NEUROD1** (panel C)	**POU2F3** (panel D)	**YAP1** (panel E)	**REST** (panel F)
Prediction **NCI**	r=0.77; p=8.8e-11	r=0.91; p=1.6e-20	r=0.86; p=1.6e-15	r=0.90; p=1.2e-18	r=0.91; p=9.3e-20	r=0.90; p=03.6e-19
Prediction **TU**	r=0.89; p=8.2e-34	r=0.93; p=1.1e-43	r=0.85; p=4.6e-28	r=0.97; p=4.2e-64	r=0.86; p=1.3e-29	r=0.93; p=2.5e-42
Prediction **UoC**	r=0.90; p=3.3e-21	r=0.94; p=1.9e-27	r=0.91; p=2.5e-22	r=0.96; p=2.0e-29	r=0.91; p=1.3e-22	r=0.94; p=1.7e-27

(r) = Pearson correlation

D

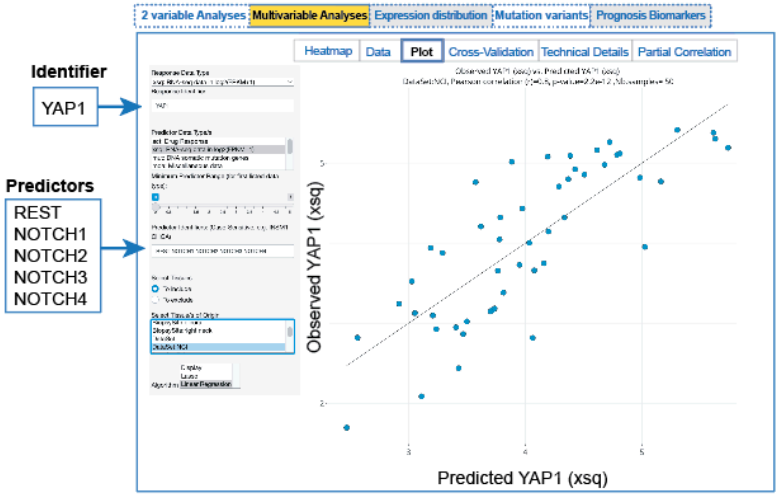

Figure S2 (related to Figs 2). **A**. Snapshot of the plot corresponding to the predictive value of the 8 variables ("Predictor Identifiers") listed in Figure 2A under "Multivariable Analyses". **B**. Snapshot of the "Technical Details" corresponding to the plot shown in panel A and the Heatmap shown in Figure 2A. **C**. Linear regression analyses for the Heatmaps shown in panels A-F of Figure 2. Pearson correlation coefficients and p-values were obtained from the "Plot" tab (as shown in panel A for Figure 2A). **D**. Expression of the Notch pathway canonical genes *REST*, *NOTCH1*, *NOTCH2*, *NOTCH3* & *NOTCH4* predict the expression of *YAP1*.

Figure S3 (related to Figure 1). **A**. Snapshot of the "Expression distribution" tab from the SCLC TumorMiner website in each of the 3 datasets of SCLC TumorMiner. Gene expression (genexp) is expressed as log2(FPKM+1). Statistical comparisons are performed by Student t-test. **** indicates $p < 0.001$; ** $p < 0.01$; * $p < 0.05$. The "Download Plot Data" tab at the bottom left enables users to export the data. **B**. Snapshot of the "Mutation Variants" tab in the SCLC TumorMiner website. Number to the right indicate the percentage of samples with deleterious mutations.

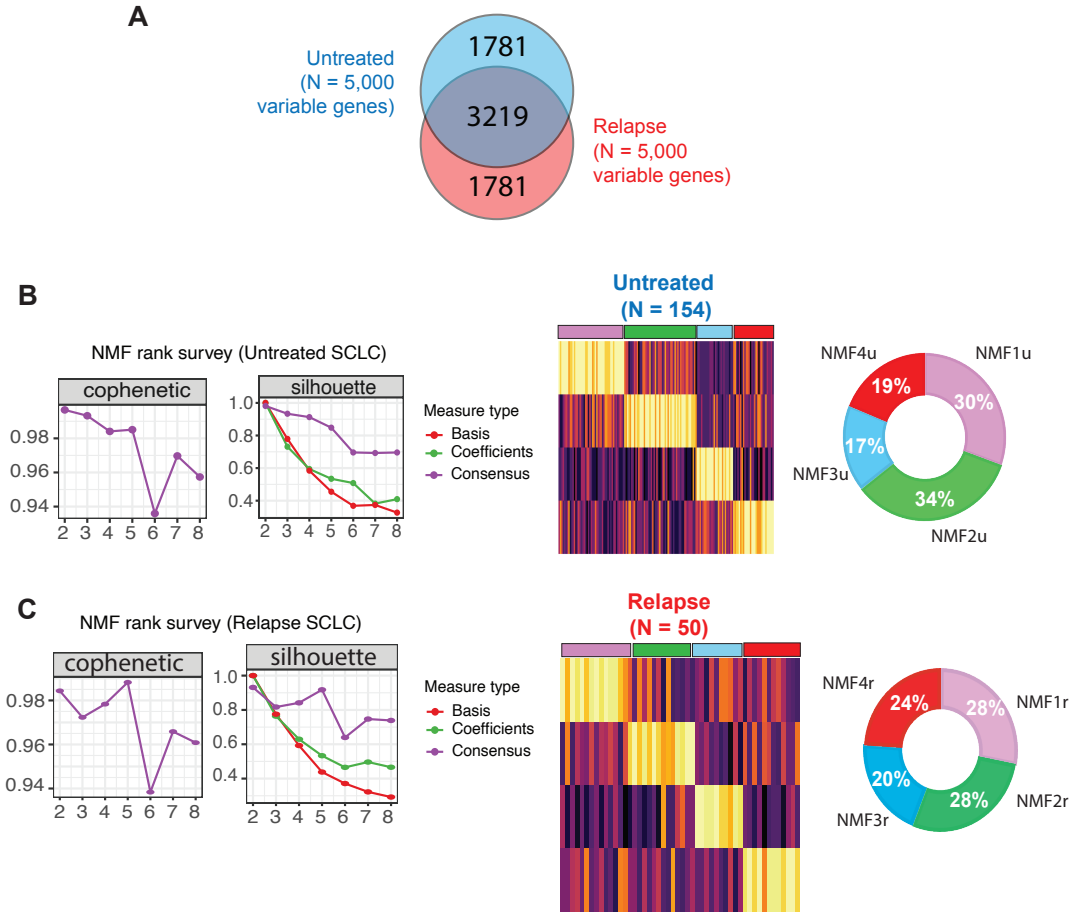

Figure S4 (related to Fig. 3). **A**. Venn-diagram showing the overlap of Untreated (top 5000) and Relapse (top 5000) most variable genes, selected using Median Absolute deviation (MAD) approach. **B** and **C** NMF rank summary for untreated and relapse SCLC samples, respectively. The cophenetic and silhouette scores are plotted for range of clusters (k=2:8), depicting k=4 as optimal number of clusters for both cohorts. Consensus matrix heatmaps at k=4 show well defined and stable clusters. Right: pie charts showing the distribution of samples in each NMF cluster.

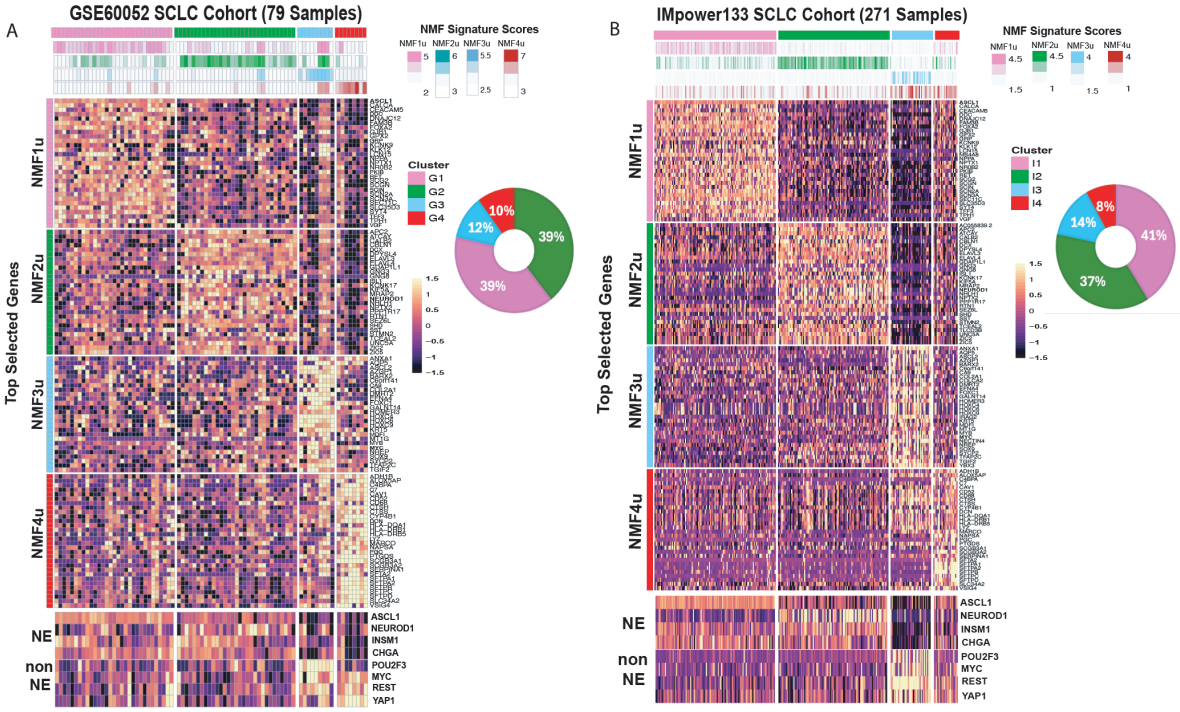

Figure S5 (related to Fig. 3): External validation of the NMFu derived gene signature on two independent SCLC cohorts (GSE60052 and Impower133). Each column represents a SCLC sample, and rows show expression of the top-30 most differentially enriched signature genes with colors indicating row-scaled expression levels. The topmost rows show 4 NMF clusters and the NMF signature scores per sample. Pie charts represent the distribution of patient samples across the different clusters.

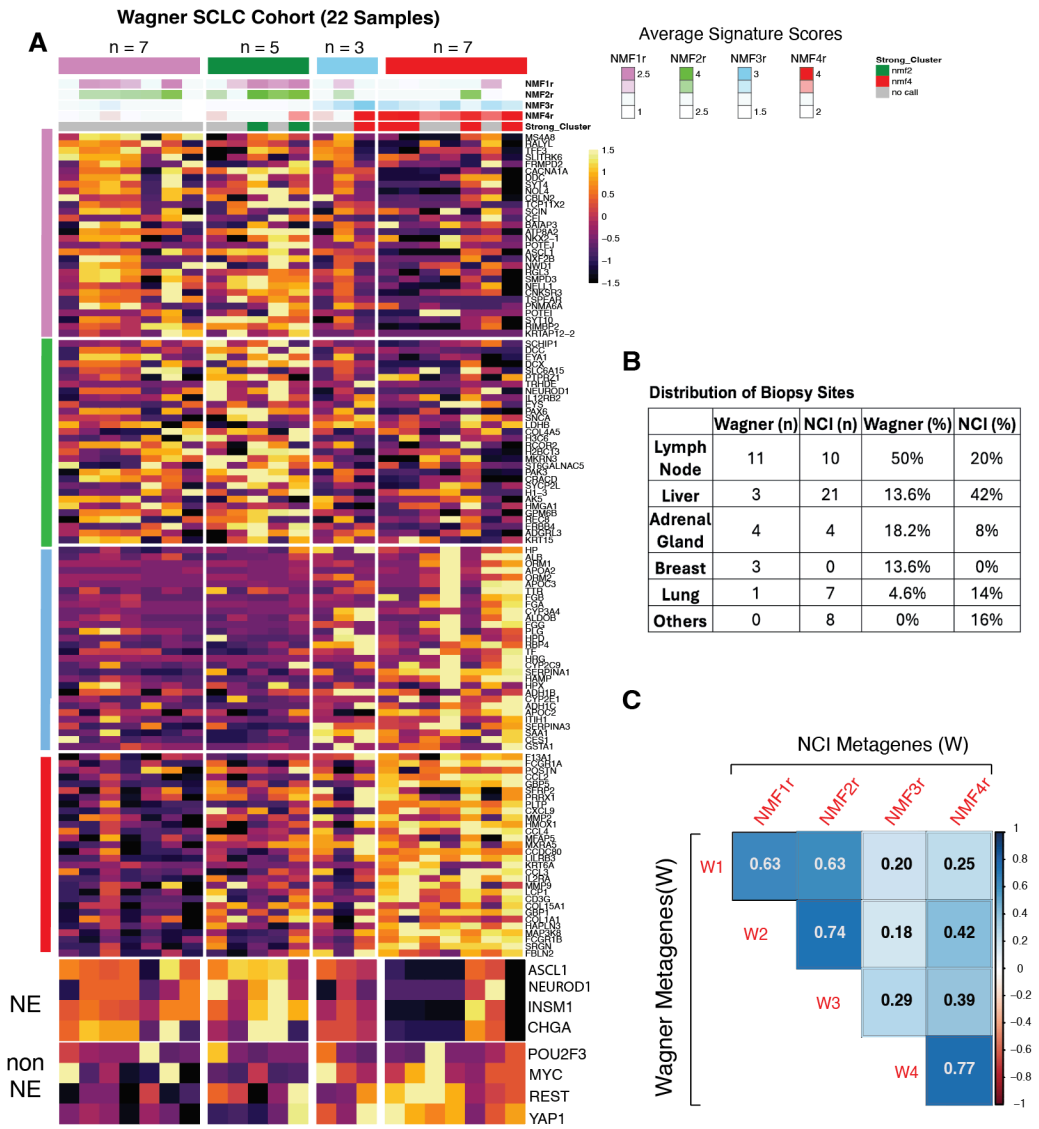

	Wagner (n)	NCI (n)	Wagner (%)	NCI (%)
Lymph Node	11	10	50%	20%
Liver	3	21	13.6%	42%
Adrenal Gland	4	4	18.2%	8%
Breast	3	0	13.6%	0%
Lung	1	7	4.6%	14%
Others	0	8	0%	16%

Figure S6 (related to Fig. 3): External validation of the NMFr-derived gene signature in an independent relapse SCLC cohort (Wagner et al. cohort) [27]. **A**. Heatmap showing the expression of the top-30 most differentially enriched genes from the NCI NMFr-derived signature across the relapse samples of the Wagner et al. cohort (n = 22). Columns represent individual tumor sample, grouped by NMF cluster assignment. Rows represent the differentially enriched gene. Colors indicate row-scaled expression levels. Top annotations display NMF cluster identity and corresponding signature scores (NMFr1–NMFr4) for each sample. Bottom annotations indicate neuroendocrine (NE) and non-NE classification based on canonical markers (including *ASCL1*, *NEUROD1*, *POU2F3*, *YAP1*). **B**. Biopsy sites in the Wagner and the NCI cohorts. **C**. Concordance between the Wagner et al. cohort subgroups and NCI metagenes for each of the NMFr. Heatmap shows correlation coefficients between Wagner NMF metagene signatures (rows; W1–W4) and the NCI metagene signatures (columns; NMF1r-NMF4r), demonstrating cross-cohort reproducibility of transcriptional subtypes.

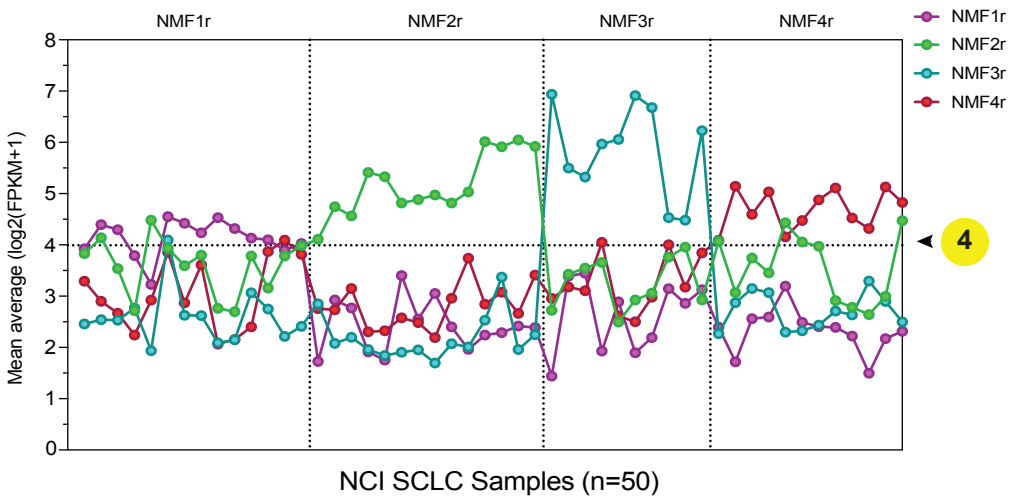

Figure S7 (related to Fig. 7). Mean average NMF expression for each and all 50 samples from patients at relapse. A mean average threshold value log2(FPKM+1) > 4 is sufficient to assign each sample to one of the 4 NMFs. The gray area defines non-significant values.

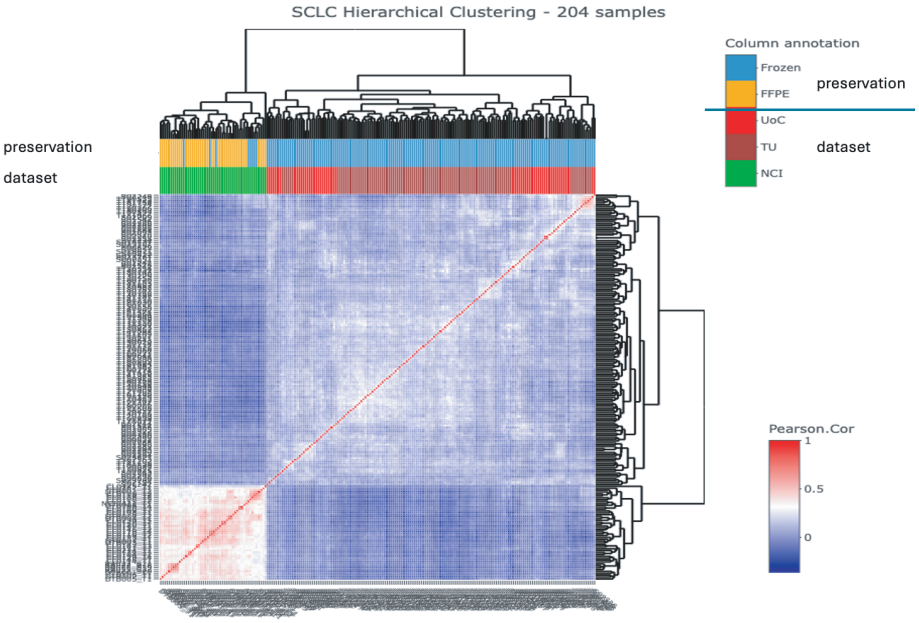

Figure S8: Hierarchical clustering of SCLC samples. The clustering shows a clear separation between NCI relapse samples (colored green) and untreated samples (TU, brown; UoC, red), as indicated in the first annotation row (sample type). The second annotation row (preservation method) shows that most NCI relapse samples are FFPE (orange), whereas all untreated samples are frozen (light blue). Because the preservation method is confounded with sample type (relapse vs. untreated), its effect cannot be disentangled.